

Chapter 5

Underwater granular flows

5.1 Introduction

Avalanches, landslides, and debris flows are geophysical hazards, which involve rapid mass movement of granular solids, water, and air as a single phase system. Globally, landslides cause billions of pounds in damage, and thousands of deaths and injuries each year. Hence, it is important to understand the triggering mechanism and the flow evolution. The momentum transfer between the discrete and the continuous phases significantly affects the dynamics of the flow as a whole (Topin et al., 2012). Although certain macroscopic models are able to capture the simple mechanical behaviours (?), the complex physical mechanisms occurring at the grain scale, such as hydrodynamic instabilities, formation of clusters, collapse, and transport (?), have largely been ignored. In particular, when the solid phase reaches a high volume fraction, the strong heterogeneity arising from the contact forces between the grains, and the hydrodynamic forces, are difficult to integrate into the homogenization process involving global averages.

In order to describe the mechanism of immersed granular flows, it is important to consider both the dynamics of the solid phase and the role of the ambient fluid (?). The dynamics of the solid phase alone are insufficient to describe the mechanism of granular flows in fluid. It is important to consider the effect of hydrodynamic forces that reduce the weight of the solids inducing a transition from dense-compacted to dense-suspended flows, and the drag interactions which counteract the movement of the solids (?). Transient regimes characterized by a change in the solid fraction, dilation at the onset of flow and the development of excess pore-pressure, result in altering the balance between the stress carried by the fluid and that carried by the grains, thereby changing the overall behaviour of the flow.

The presence of a fluid phase in a granular medium has profound effects on its mechanical behaviour. In dry granular media, the rheology is governed by grain inertia and static stresses

sustained by the contact network depending on the shear-rate and the confining pressure, respectively (?). As the fluid inertia and viscosity come into play, complications arise as a result of contradictory effects. On one hand, the fluid may delay the onset of granular flow or prevent the dispersion of the grains by developing negative pore-pressure (??). On the other hand, the fluid lubricates the contacts between grains, enhancing the rate of granular flow, but it has a retarding effect at the same time by inducing drag forces on the grains. The objective of the present study is to understand the differences in the mechanism of flow initiation and kinematics between dry and submerged granular flows. In the present study, a coupled 2D Lattice-Boltzmann and Discrete Element Method is used to model the fluid-soil interactions in underwater granular flows. The choice of a 2D geometry has the advantage of cheaper computational effort than a 3D case, making it feasible to simulate very large systems. The configuration and parameters studied in this chapter are presented in table 5.1.

5.2 LBM-DEM permeability

In a 3D granular assembly, the pore spaces between the grains are interconnected, whereas in a 2-D assembly, a non-interconnected pore-fluid space is formed as the grains are in contact with each other. This means that the fluid enclosed between the grains cannot flow to the neighbouring pore-spaces. This results in an unnatural no flow condition in a 2-D case (figure 5.1). In order to overcome this effect, a reduction in radius is assumed only during the LBM computation (fluid and fluid – solid interaction) steps. The reduced radius of the soil grain, i.e., the *hydrodynamic radius* r , allows for interconnected pore space through which the pore-fluid can flow similar to the 3D behaviour. The reduction in the radius is assumed only during LBM computations, hence this technique has no effect on the grain – grain interactions computed using DEM.

Realistically, the hydrodynamic radius can be varied from $r = 0.7R$ to $0.95R$, where R is the grain radius. Different permeabilities can be obtained for any given initial packing by varying the hydrodynamic radius of the grains, without having to change the actual granular packing. This introduces a new parameter into the system. In a physical sense, a hydrodynamic radius represents the three-dimensional permeability of a granular assembly simulated as a two-dimensional geometry.

Table 5.1 Configurations for LBM-DEM simulations of granular collapse in fluid

Simulations	Aspect ratio	Hydrodynamic radius	Packing density (%)	Slope angle (°)
Collapse on a horizontal surface				
Effect of initial aspect ratio	0.2 - 6	r = 0.7 R	83	0
Effect of permeability	0.2 - 6	r = 0.7, 0.75, 0.8, 0.85, 0.9 & 0.95 R	83	0
Effect of initial density	0.8	r = 0.7, 0.75, 0.8, 0.85, 0.9 & 0.95 R	79 & 83	0
Collapse on an inclined plane				
Effect of initial density	0.8	r = 0.9 R	79 & 83	0, 2.5, 5 & 7.5
Effect of permeability	0.8	r = 0.7, 0.75, 0.8, 0.85 & 0.9 R	79 & 83	0 & 5
Tall columns	6	r = 0.85 R	79 & 83	0, 2.5, 5 & 7.5

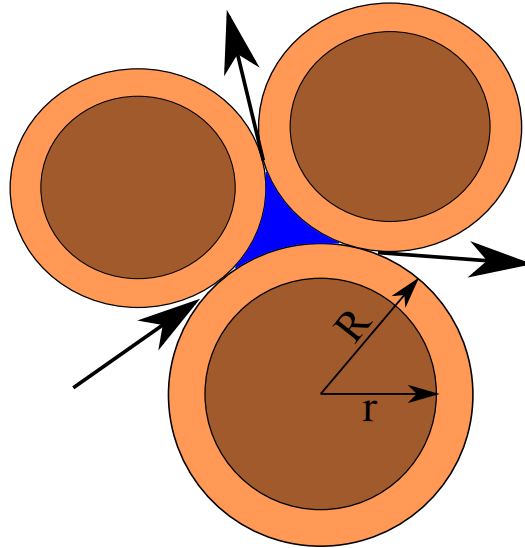


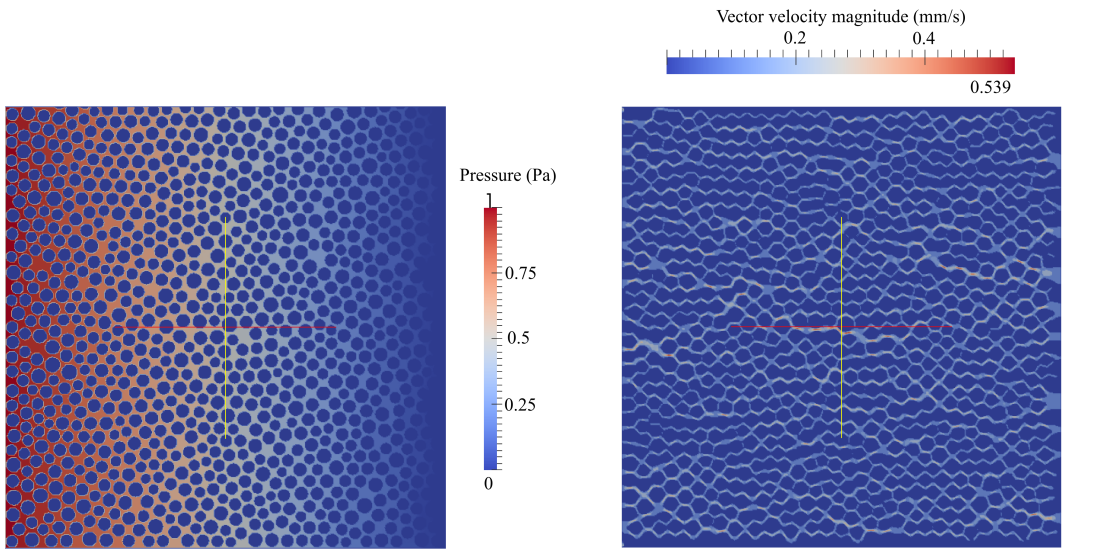
Figure 5.1 Schematic representation of the hydrodynamic radius in LBM-DEM computation.

The hydrodynamic radius can also be assumed to represent the irregularities on the granular surface. The hydrodynamic radius represents asperities on the grain surface, which represents a channel for the fluid to flow between the grains.

In order to understand the relation between the hydrodynamic radius and the permeability of the granular assembly, horizontal permeability tests are performed by varying the hydrodynamic radius as $0.7 R$, $0.75 R$, $0.8 R$, $0.85 R$, $0.9 R$ and $0.95 R$. A square sample of $50 \text{ mm} \times 50 \text{ mm}$ filled with poly-disperse ($d_{\max}/d_{\min} = 1.8$) grains having a mean diameter of 1.7 mm is used to determine the relation between the hydrodynamic radius and the permeability. Dirichlet boundary condition (discussed in ??), i.e., density constraint, is applied along the left and the right boundaries of the sample. The fluid density on the left boundary is increased in small steps ($10^{-4} \Delta P$), while a constant density is maintained on the right boundary. This results in a pressure gradient causing the fluid to flow (figure 5.2) through the pore-space.

For a given hydrodynamic radius, the pressure gradient ΔP is varied to obtain different flow rates. Probing the fluid space showed a Poiseuille flow behaviour between the grains. The flow is still within the Darcy's laminar flow regime, which is verified by the linear slope between the pressure gradient and the mean flow velocity (figure 5.3). From the mean flow velocity (v), the transverse permeability (k) of the sample is computed as:

$$k = v \cdot \mu \cdot \frac{\Delta x}{\Delta P}, \quad (5.1)$$



(a) Pressure gradient in the granular assembly (b) Horizontal flow due to pressure gradient

Figure 5.2 Evaluation of the horizontal permeability for a hydrodynamic radius of 0.7 R.

where μ is the dynamic viscosity of the fluid (Pa s), Δx is the thickness of the bed of porous medium m, and ΔP is the applied pressure difference Pa. It can be observed that with increase in the hydrodynamic radius the permeability decreases, i.e., the slope of the mean flow velocity to the pressure gradient decreases. At very low pressure gradients ($\Delta P \leq 0.1$), both 0.9 R and 0.95 R have no flow. Even at higher pressure gradients, a hydrodynamic radius of $r = 0.95R$ shows almost no flow behaviour. A high value of hydrodynamic radius $r > 0.95R$ results in unnatural flow/no-flow behaviour. Hence in the present study, a hydrodynamic radius in the range of 0.7 to 0.95 R is adopted.

Increase in the hydrodynamic radius from 0.7 to 0.95 reduces the porosity from 0.60 to 0.27. The permeability computed from LB – DEM method is verified by comparing it with the analytical solution. One of the widely used analytical solution for permeability is the Carman – Kozeny equation (CK Model), which is based on the Poiseuille's flow through a pipe and is mainly used for 3D, homogeneous, isotropic, granular porous media at moderate porosities. In the present study, a modified Carman – Kozeny equation that takes into account of the micro-structure of the fibres and that is valid in a wide range of porosities is adopted (?). The normalized permeability is defined as

$$\frac{k}{d^2} = \frac{\varepsilon}{\psi_{CK}(1 - \varepsilon)^2}. \quad (5.2)$$

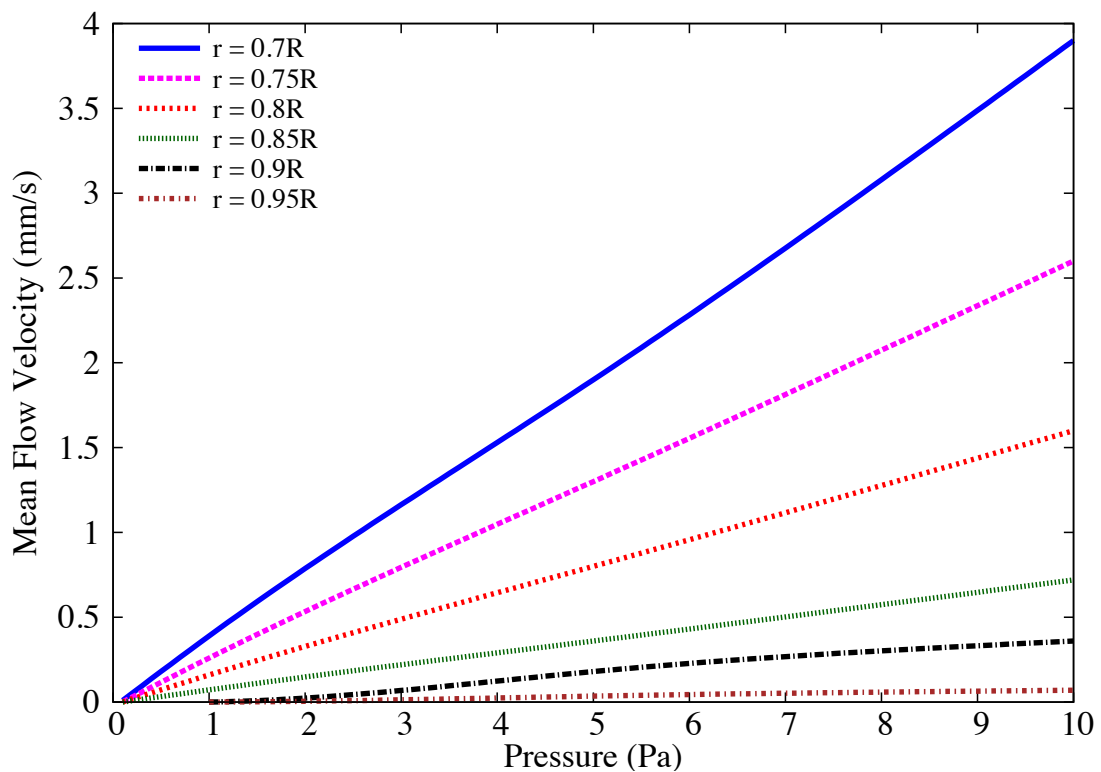


Figure 5.3 Variation of the mean flow velocity with pressure gradient for different hydrodynamic radius.

In the CK model, the hydraulic diameter D_h , is expressed as a function of measurable quantities: porosity and specific surface area

$$D_h = \frac{4\epsilon V}{S_v} = \frac{\epsilon d}{(1-\epsilon)}, \quad (5.3)$$

$$a_v = \frac{\text{grain surface}}{\text{grain volume}} = \frac{S_v}{(1-\epsilon)V} = \frac{4}{d}, \quad (5.4)$$

where S_v is the total wetted surface, and a_v is the specific surface area. The above value of a_v is for circles (cylinders) - for spheres $a_v = 6/d$. ψ_{CK} is the empirically measured CK factor, which represents both the shape factor and the deviation of flow direction from that in a duct. It is approximated for randomly packed beds of spherical grains. The variation of normalized permeability with porosity, obtained by varying the radius from 0.7 R to 0.95 R, is presented in figure 5.4. The permeability values obtained from LBM - DEM simulations are found to match the qualitative trend of the Carman-Kozeny equation. The LB - DEM permeability curve lies between the permeability curves for spherical and cylindrical grain arrangements implying a better simulation of three-dimensional permeability using a 2D granular assembly. Thus using a hydrodynamic radius, realistic 3D fluid - grain interactions can be simulated in a 2D geometry.

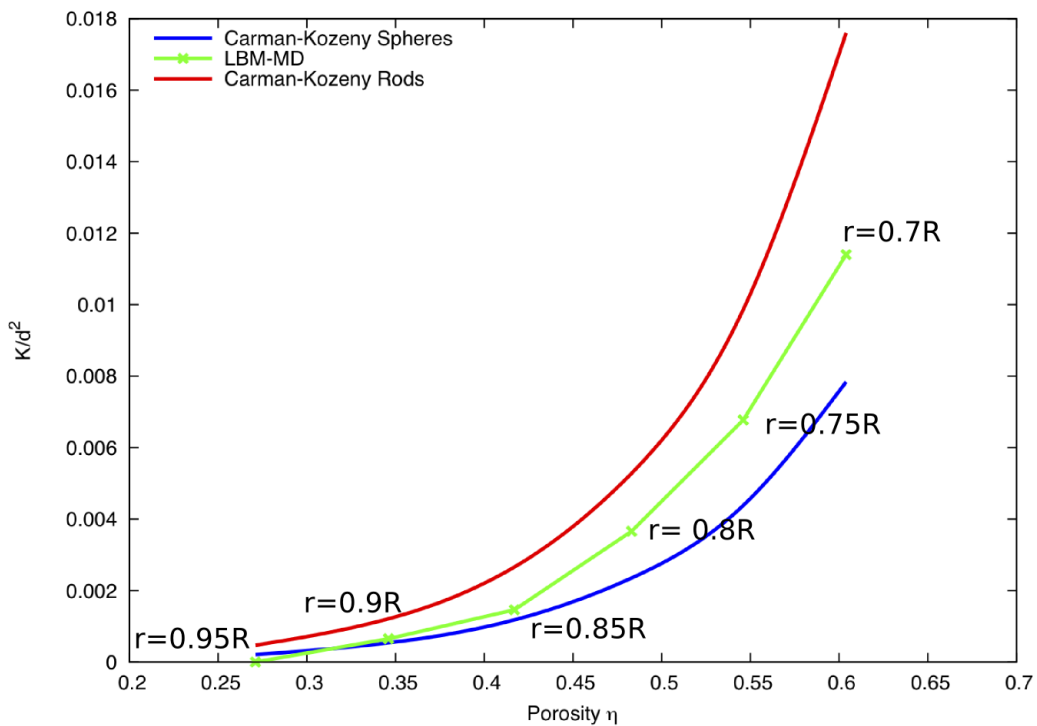


Figure 5.4 Relation between permeability and porosity for different hydrodynamic radius and comparison with the analytical solution.

5.3 Granular collapse in fluid

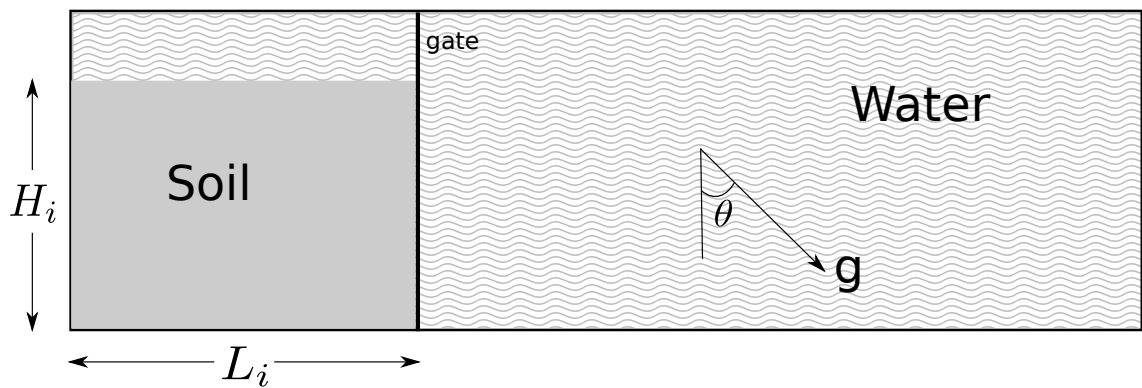
The collapse of a granular column, which mimics the collapse of a cliff, has been extensively studied in the case of dry granular material, when the interstitial fluid plays no role (section 4.2). The problem of the granular collapse in a liquid, which is of importance for submarine landslides, has attracted less attention (Rondon et al., 2011). ? observed that the presence of liquid dramatically changes the way a granular column collapses compared to the dry case. The destabilization of a granular pile strongly depends on the initial volume fraction. For dense packings the granular flow is localized at the free surface of the pile, whereas for loose packings the destabilization occurs in the bulk of the material and has a parabolic profile (???).

5.3.1 LBM-DEM set-up

In the present study, the collapse of a granular column in fluid is studied using 2D LBM - DEM. The effect of initial aspect ratio on the run-out behaviour is investigated. The flow kinematics are compared with the dry and buoyant granular collapse to understand the influence of hydrodynamic forces and lubrication on the run-out. Unlike dry column, the permeability and the initial volume fraction are expected to have a significant influence on the flow dynamics. Hence the effect of these parameters on the run-out behaviour is investigated.

The granular column collapse set-up in fluid is very similar to the dry granular column collapse. A rectangular channel of length L_0 and height H_0 is filled with poly-dispersed discs, $d_{max}/d_{min} = 1.8$ (Figure 5.5a). Once the DEM soil grains reach equilibrium in the dry condition, the granular sample is then placed in the fluid domain simulated using LBM. The LBM-DEM set-up of a granular column with an aspect ratio a of 6 in fluid is shown in figure 5.5b. The fluid has a density of 1000 kg m^{-3} and a kinematic viscosity of $1 \times 10^{-6} \text{ m}^2 \text{ s}^{-1}$. The gate supporting the right-hand side boundary of the granular column is opened allowing the column to collapse and flow in a fluid. The final run-out distance is measured as L_f and final collapse height as H_f . The collapse takes place on a horizontal surface. The initial aspect ratio of the column is varied as 0.2, 0.4, 0.6, 0.8, 1, 2, 4 and 6.

The cumulative β distribution is adopted to generate grains with d_{max} and d_{min} as 2.2 mm and 1.25 mm, respectively. The soil column is modelled using ~ 2000 discs of density 2650 kg m^{-3} and a contact friction angle of 26° . A linear-elastic contact model is used in the DEM simulations. The granular assembly has a packing fraction of 83%. The critical time step for DEM is computed based on the local contact natural frequency and damping ratio. A sub-cycling time integration is adopted in DEM (??). A fluid flow (LBM) time step of $\Delta t = 2.0 \times 10^{-5} \text{ s}$ is determined based on the viscosity and the relaxation parameter



(a) Schematic view of underwater granular collapse set-up.

(b) LBM-DEM simulation of underwater granular collapse set-up ($a = 6$).

Figure 5.5 Underwater granular collapse set-up.

$\tau = 0.506$. An integer ratio n_s , between the fluid flow time step Δt and the DEM time step Δt_D is determined as 15, i.e., every LBM iteration involves a sub-cycle of 15 DEM iterations.

In order to capture the realistic physical behaviour of the fluid – grain systems, it is essential to model the boundary condition between the fluid and the grain as a non-slip boundary condition, i.e. the fluid near the grain should have similar velocity as the grain boundary. The solid grains inside the fluid are represented by lattice nodes. The discrete nature of the lattice results in a stepwise representation of the surfaces (figure 5.6), which are otherwise circular, hence sufficiently small lattice spacing h is required. The smallest DEM grain in the system controls the size of the lattice. In the present study, a very fine discretisation of $d_{min}/h = 10$ is adopted, i.e., the smallest grain with a diameter d_{min} in the system is discretised into 100 lattice nodes ($10h \times 10h$). This provides a very accurate representation of the interaction between the solid and the fluid nodes. A hydrodynamic radius of 0.7 R is adopted during the LBM computations. The fluid pressure on the top and right boundaries are maintained constant. Hence, any pressure wave that is generated during the collapse is absorbed in the boundary. Frictional boundary constraint is applied along the bottom boundary.

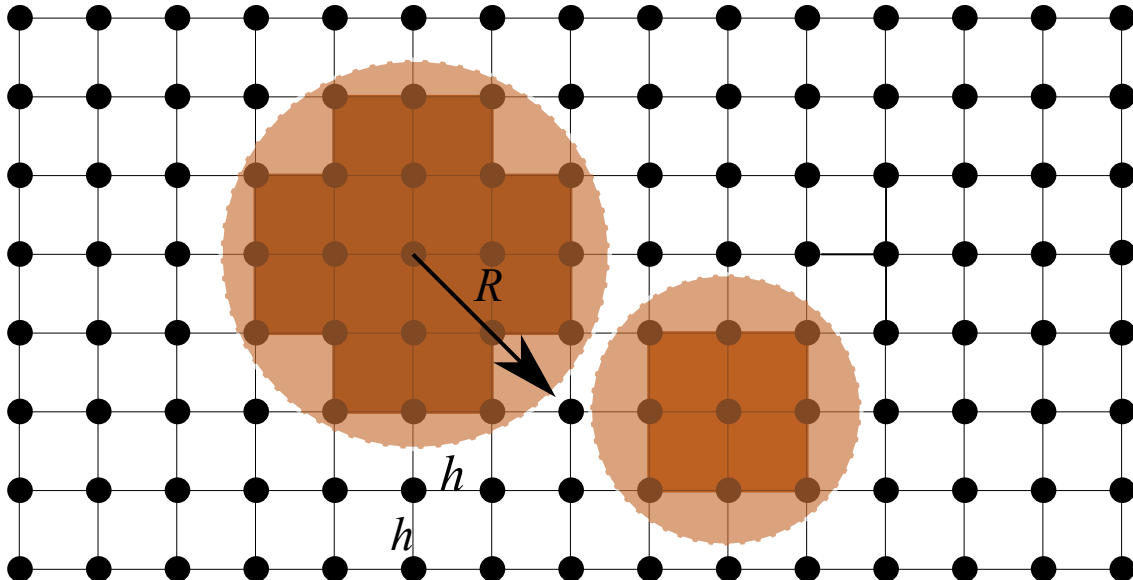


Figure 5.6 Discretisation of solid grains in LBM grid. Shows the step-wise representation of circular disks in the lattice.

5.3.2 Collapse in fluid: Flow evolution

Two-dimensional plane-strain LBM-DEM simulations of granular column collapse are performed by varying the initial aspect ratio of the column from 0.2 to 6. The normalized

final run-out distance is measured as $\Delta L = (L_f - L_0)/L_0$. Similar to the dry granular collapse, the duration of collapse is normalised with a critical time $\tau_c = \sqrt{H/g}$, where H is the initial height of the granular column and g is the acceleration due to gravity. Dry and buoyant analyses of granular column collapse are also performed to understand the effect of hydrodynamic forces on the run-out distance.

Snapshots of the flow evolution of a granular column collapse with an initial aspect ratio of 0.4 are shown in figure 5.7. The failure begins at the toe end of the column, and the fracture surface propagates into the column at an angle of about 50° , similar to the dry column collapse. For the short column, the failure is due to collapse of the flank. Once the material is destabilised, the granular mass interacts with the surrounding fluid resulting in formation of turbulent vortices. These vortices interact with the grains at the surface resulting in irregularities on the free surface. Force chains can be observed in the static region of collapse, which indicates the flow can be described using a continuum theory. As the granular material ceases to flow, force chains develop at the flow front, revealing consolidation of the granular mass resulting in an increase in the shear strength.

The evolution of run-out with time for a short column ($a = 0.4$) is presented in figure 5.8a. The dry column exhibits longer run-out distance in comparison to the submerged column. The collapse of a dry column using DEM represents a collapse in a vacuum, without any influence of drag forces or viscosity of air. A LBM-DEM simulation of a granular column collapse using the kinematic viscosity of air is performed to compare the dry column with the collapse in air. Although the effect of viscous drag can be observed in the collapse in the air, both the “dry” condition and the collapse in air show almost the same run-out behaviour. However, the collapse in fluid (water) results in a much shorter run-out distance. The granular mass in fluid has the buoyant mass, in contrast to the dry density. A dry granular collapse with the buoyant unit weight also exhibits longer run-out behaviour than the collapse in fluid. However, due to decrease in the initial potential energy, the run-out observed in the buoyant condition is shorter than the dry condition. The column collapse in fluid takes longer to evolve, which might be due to the development of large negative pore water pressure that is generated during the shear failure along the fracture surface. This large negative pore-pressure has to be dissipated before the granular mass, above the fracture surface, can collapse and flow. The shorter run-out distance in the fluid case, in comparison with the dry and buoyant conditions, shows that the collapse in fluid is significantly affected by the hydrodynamic drag forces acting on the soil grains. The evolution of height H/L is presented in figure 5.8b. Since the failure of the column is only at the flank, the central static region remains unaffected. Hence, the final height of the column is the same in dry and submerged conditions.

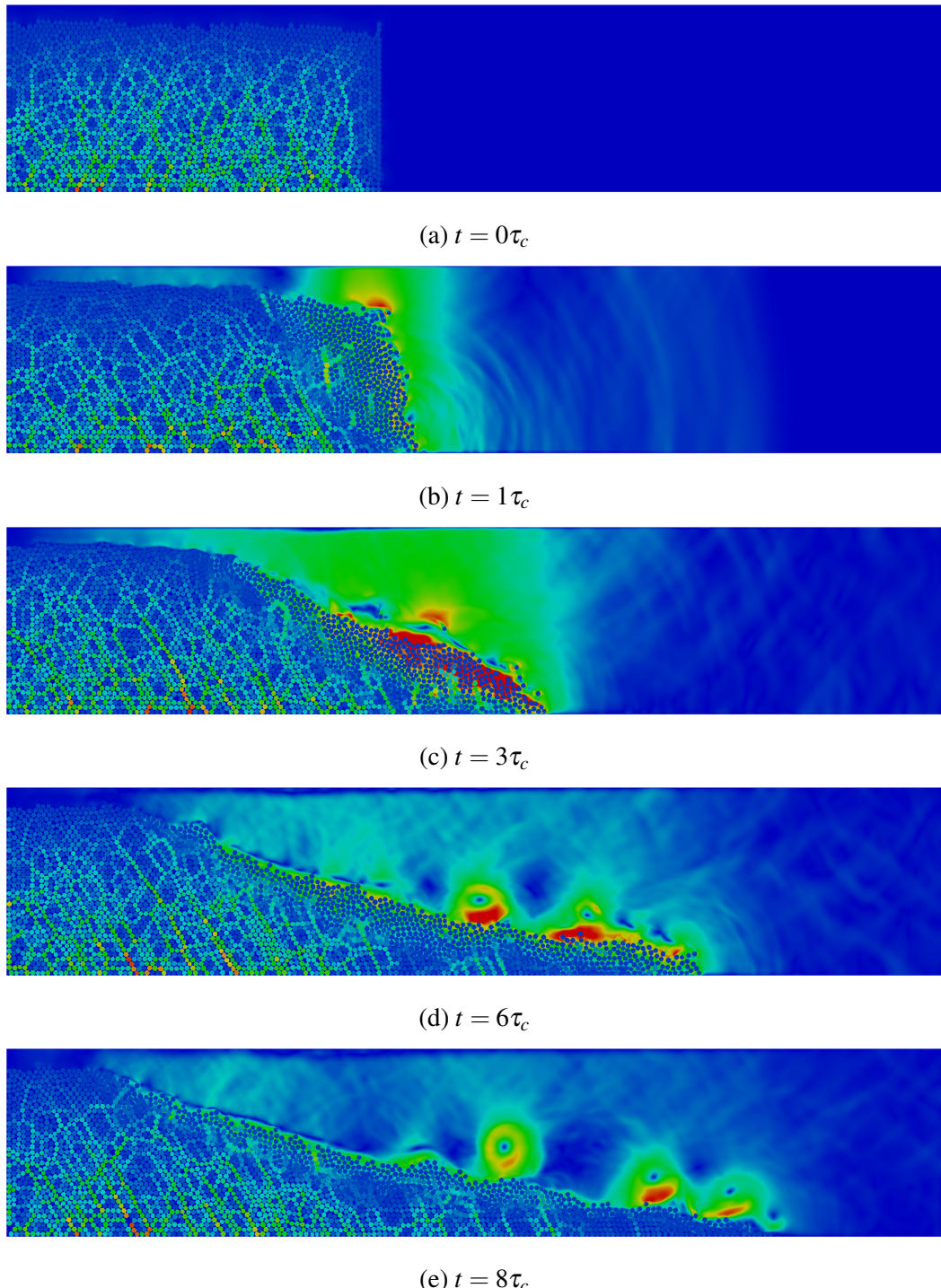


Figure 5.7 Flow evolution of a granular column collapse in fluid ($a = 0.4$). Shows the velocity profile of fluid due to interaction with the grains (red - higher velocity).

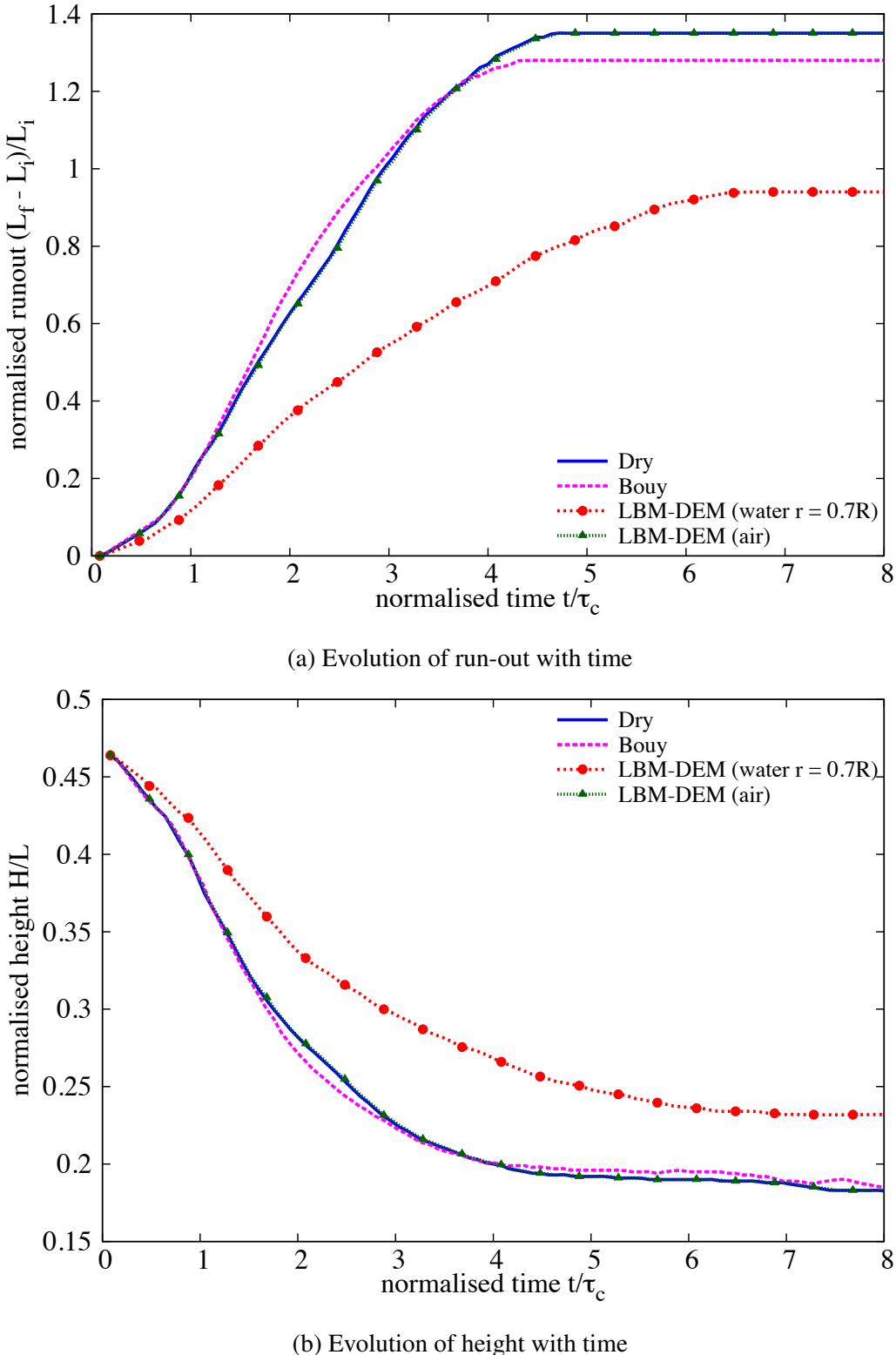


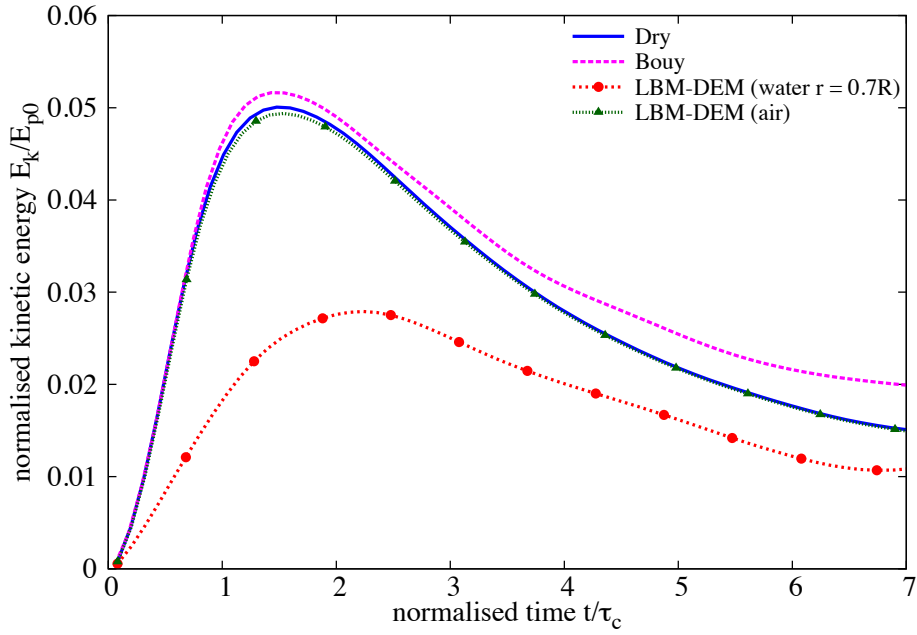
Figure 5.8 Evolution of height and run-out with time for a column collapse in fluid ($a = 0.4$).

The evolution of the normalised kinetic energy with time for a column with an initial aspect ratio of 0.4 is shown in figure 5.9. It can be observed that the peak kinetic energy is attained later in the submerged condition than the dry collapse. This can be attributed to the time required to overcome the negative pore-pressure generated during the shear along the fracture surface. For short columns the critical time τ_c is controlled by the vertical kinetic energy. The amount of kinetic energy in submerged case is significantly lower than the dry condition. Also, the potential energy evolution (figure 5.10) shows a significant influence of the hydrodynamic forces on the amount of material destabilised during the collapse. The drag forces on the soil grains reduce and slow down the amount of material that undergo collapse resulting in a shorter run-out distance for short columns.

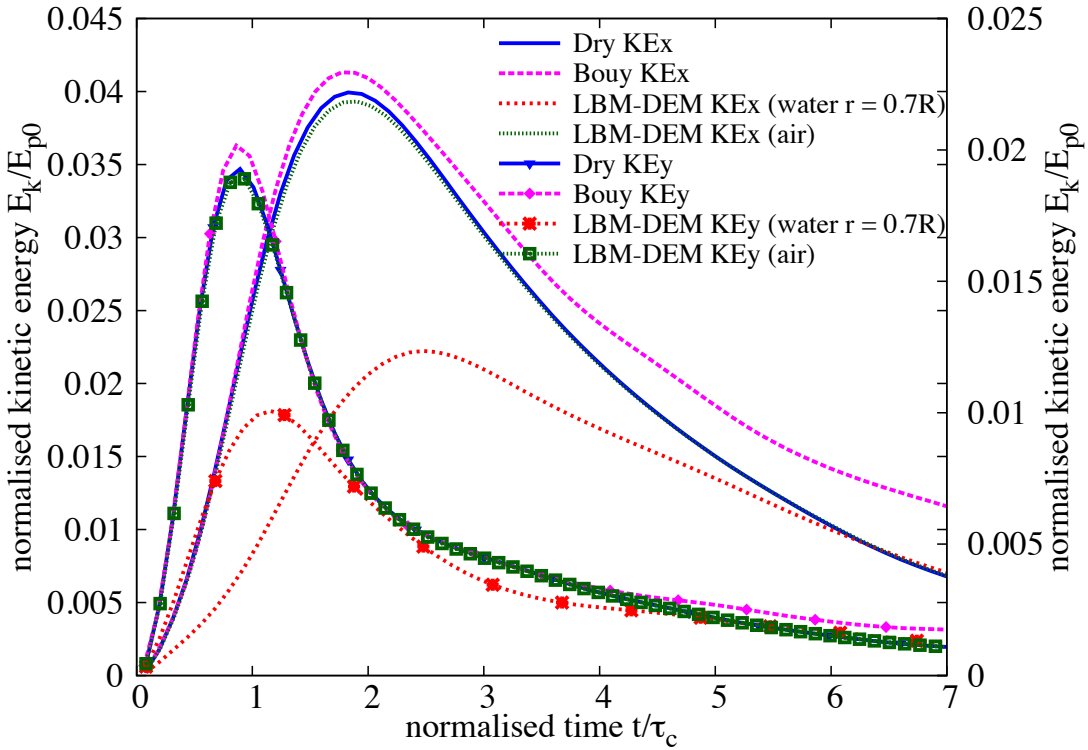
Snapshots of the flow evolution of a granular column collapse with an initial aspect ratio of 4 is shown in figure 5.11. For a tall column, the collapse mechanism changes. The entire column is involved in the collapse. The height of the static region, which is below the fracture surface, is shorter than the total height of the column. This results in a free-fall of grains above the fracture surface. As the grains experience free-fall they interact with the surrounding fluid. However, no vortices are observed during the initial stage of collapse. In the second phase, when the grains reach the base, the vertical acceleration gained during the free-fall is converted into horizontal velocity. As the grains are ejected horizontally, the free surface of the granular mass interacts with the fluid resulting in the formation of turbulent vortices. Unlike short columns, these vortices have significant influence on the mass distribution along the run-out. Heaps of granular material can be observed in front of each vortex. The number of vortices formed during a collapse is found to be proportional to the amount of material destabilised, i.e., the length of free-surface interacting with the fluid influences the number of vortices generated during the collapse. The reappearance of force chains at $t = 6\tau_c$ and $8\tau_c$ indicates the granular mass is consolidating resulting in an increase in the shear strength.

The time evolution of the run-out and the height of a tall column ($a = 4$) is presented in figure 5.12a and figure 5.12b, respectively. Similar to the short column, the run-out observed in the dry condition is much longer than that observed in the submerged condition. Also, the evolution of run-out is slower in the case of submerged condition, which indicates the influence of drag force on the run-out evolution. The height of the column is strongly influenced by the hydrodynamic forces (figures 5.12b and 5.13), which reduces the amount of material destabilised during the collapse.

The evolution of kinetic energies with time for an initial aspect ratio 4 is presented in figure 5.14. Even during the free-fall stage, the peak vertical kinetic energy is delayed in the case of fluid, which shows the influence of viscosity on the flow evolution. Almost



(a) Evolution of the total kinetic energy.



(b) Evolution of horizontal and vertical kinetic energies.

Figure 5.9 Evolution of kinetic energies with time for a granular column collapse in fluid ($a = 0.4$)

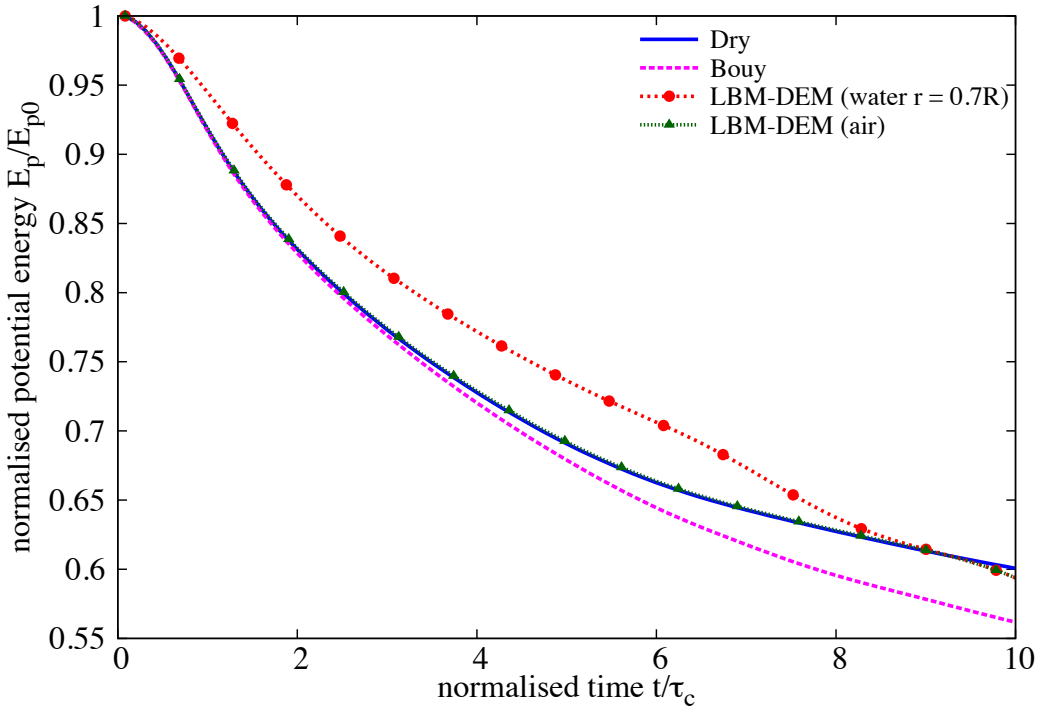


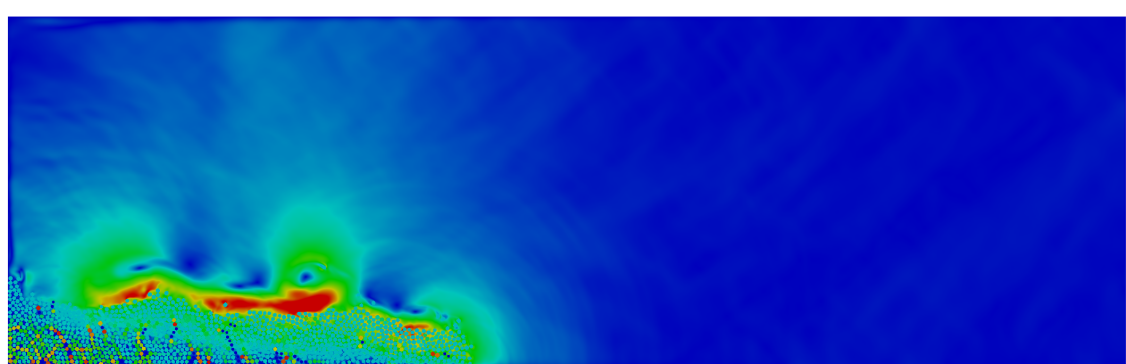
Figure 5.10 Evolution of the potential energy with time for a granular column collapse in fluid ($a = 0.4$)

half of the kinetic energy that is available in the case of dry granular collapse is dissipated through the drag forces experienced by the grains. This shows that the influence of viscous drag on the run-out evolution is significantly higher than the effect of lubrication.

The final run-out distance as a function of the initial aspect ratio of the column is presented in figure 5.15a. For all aspect ratios, the run-out observed in the dry case is significantly higher than the submerged condition. For short columns, the run-out distance is found to be have a linear relationship with the initial aspect ratio of the column. A power law relation is observed between the run-out and the initial aspect ratio of the column.

$$\frac{L_f - L_0}{L_0} \propto \begin{cases} a, & a \lesssim 2.7 \\ a^{2/3}, & a \gtrsim 2.7 \end{cases} \quad (5.5)$$

The normalised final height as a function of the initial aspect ratio of the column is presented in figure 5.15b. It can be observed that the final collapse height is much higher in the submerged condition than the dry condition. The drag force on the granular column reduces the amount of collapse, resulting in a shorter run-out distance. The drag force seems to have a predominant influence on the run-out behaviour than the lubrication effect in fluid.

 $t = 0\tau_c$  $t = 1\tau_c$  $t = 3\tau_c$

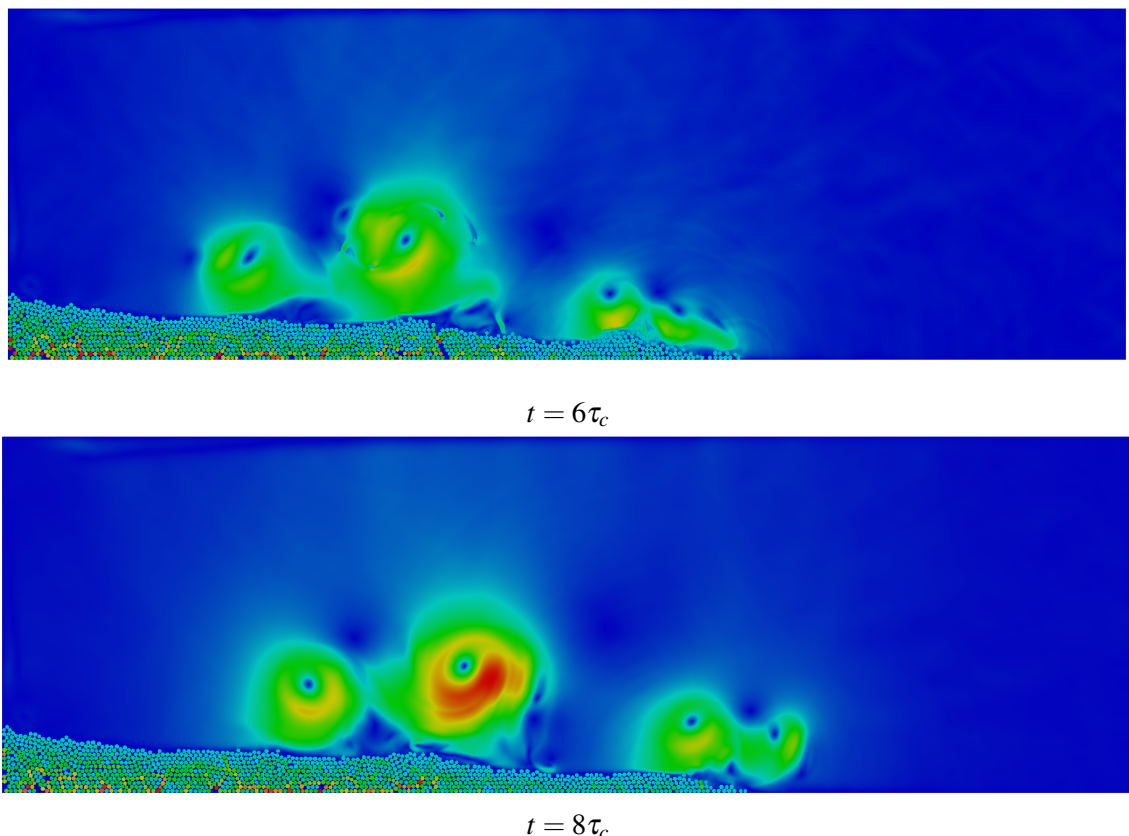


Figure 5.11 Flow evolution of a granular column collapse in fluid ($a = 4$). Shows the velocity profile of fluid due to interaction with the grains (red - higher velocity).

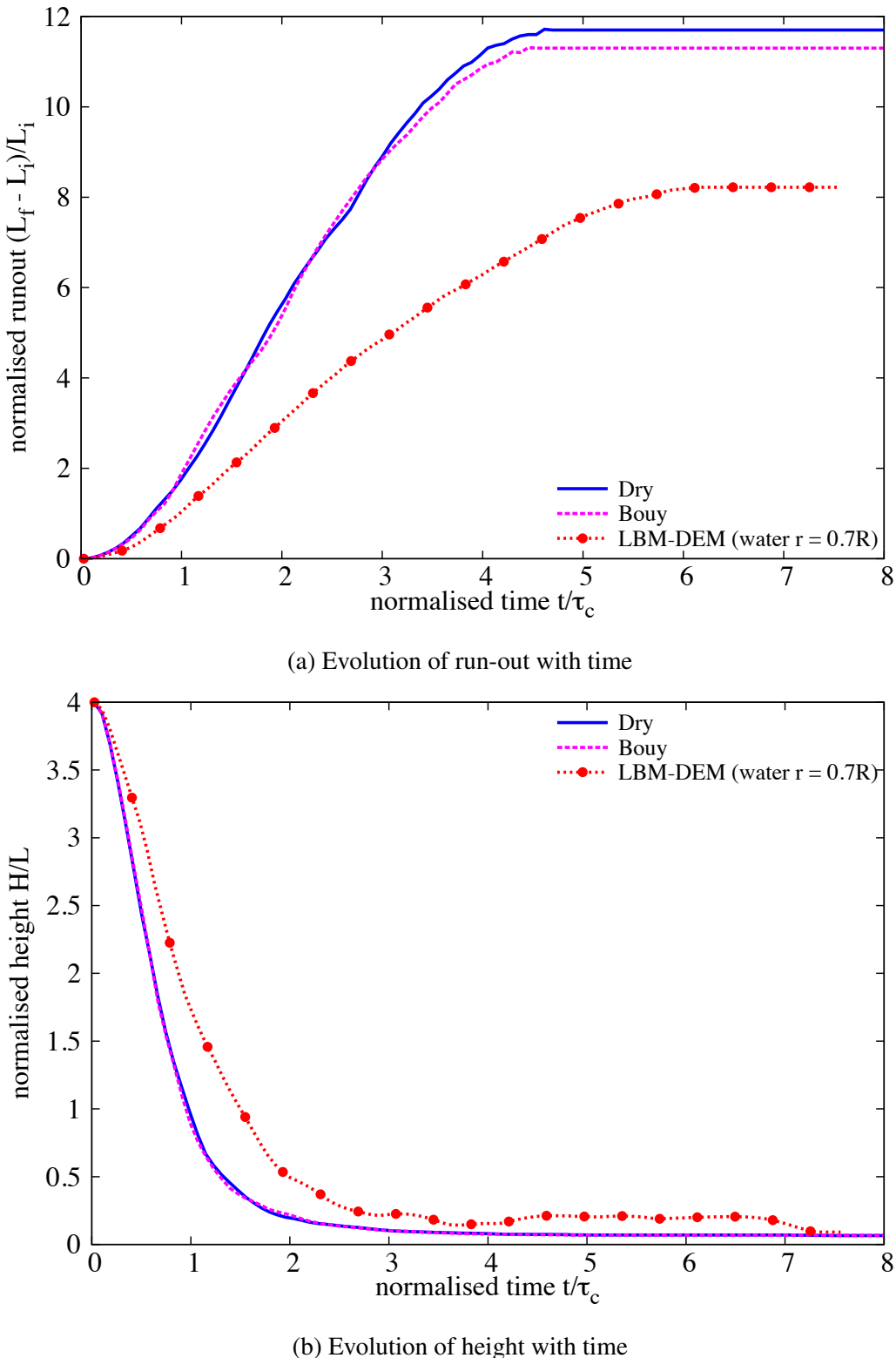


Figure 5.12 Evolution of run-out and height with time for a column collapse in fluid ($a = 4$)

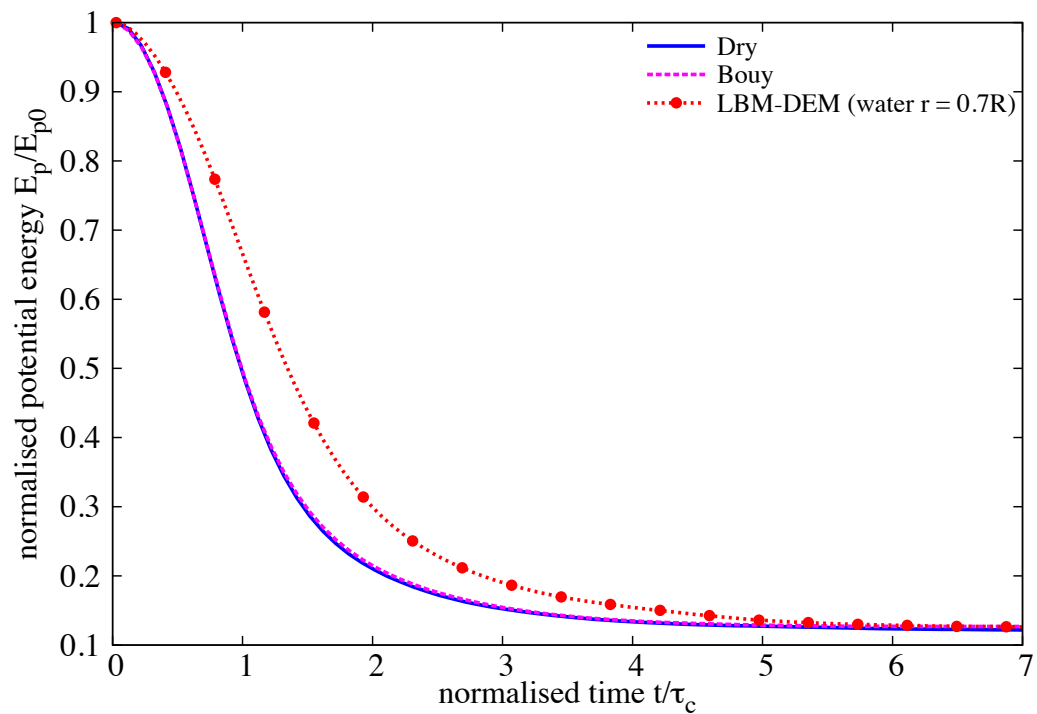


Figure 5.13 Evolution of the potential energy with time for a granular column collapse in fluid ($a = 4$)

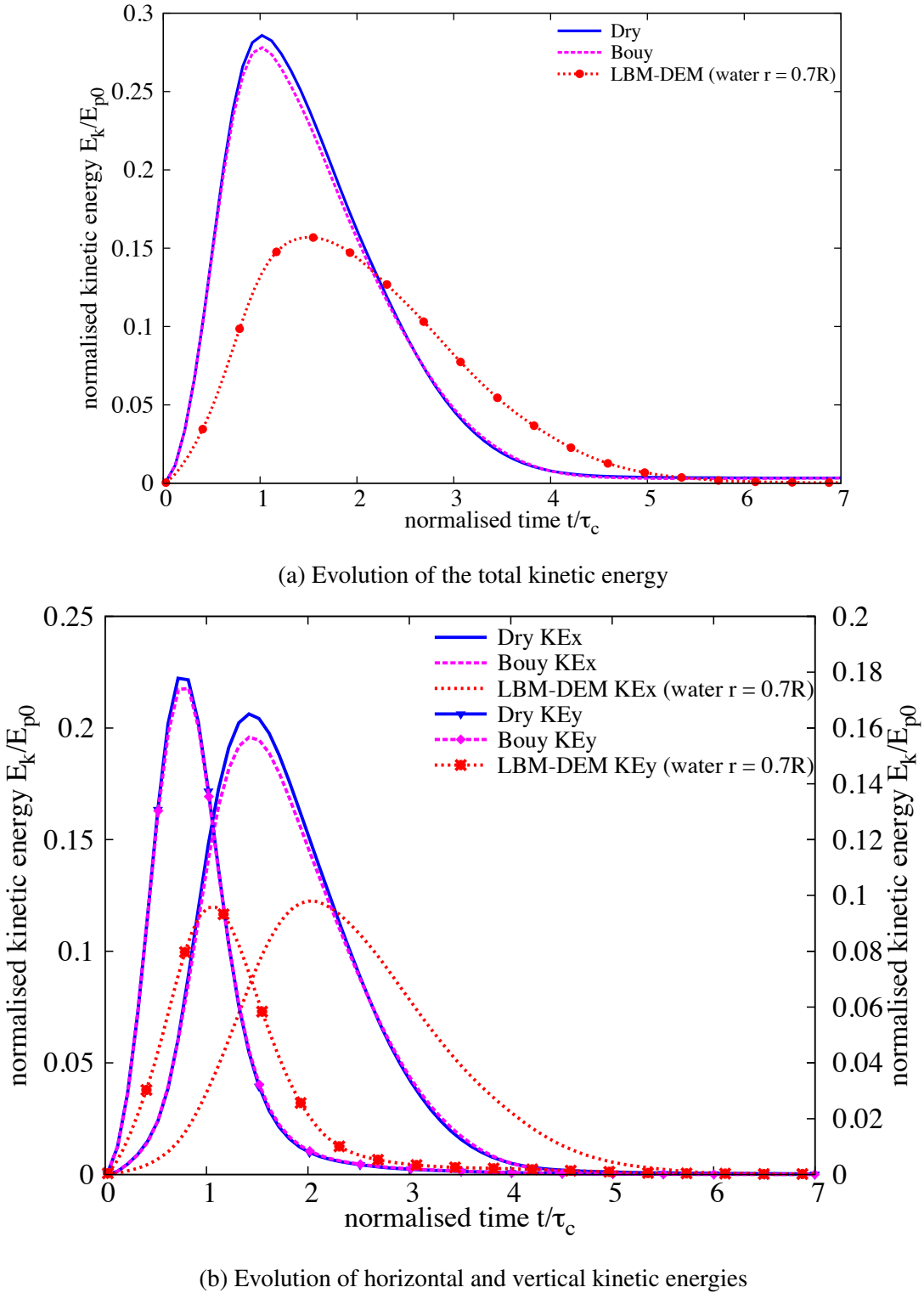
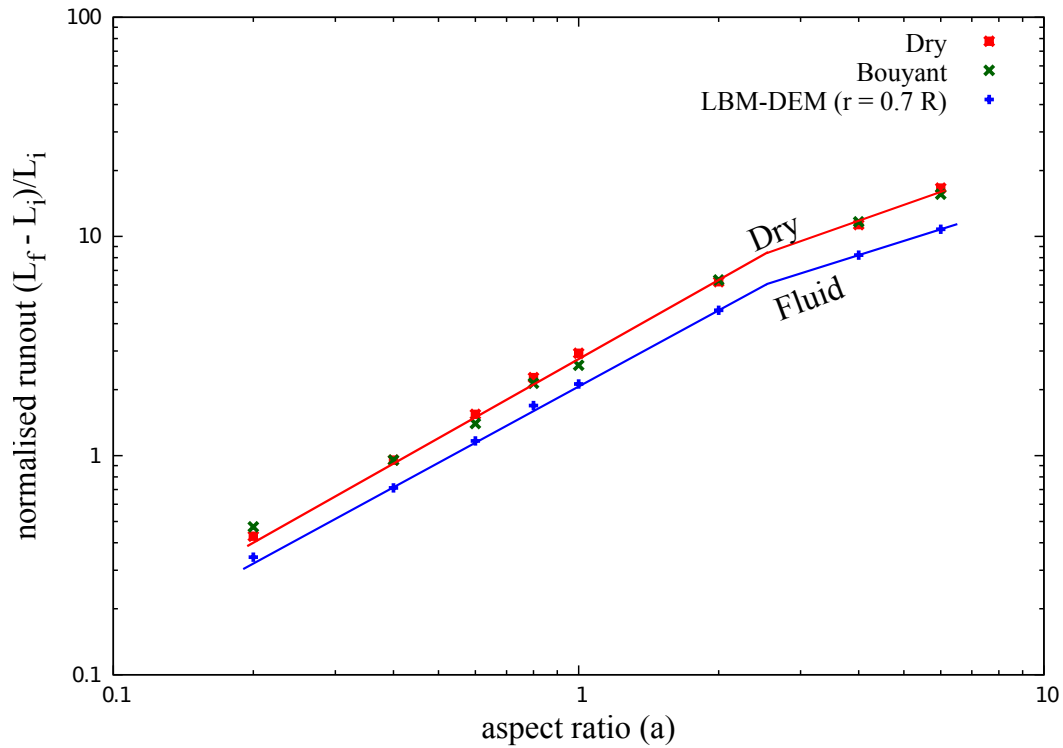
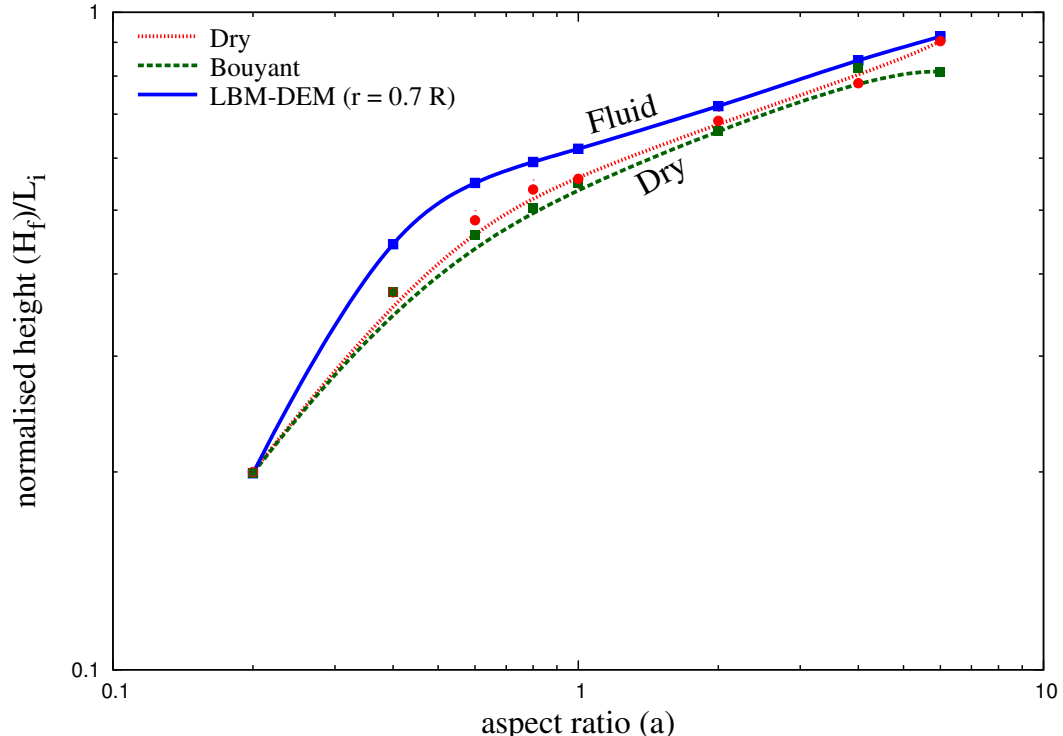


Figure 5.14 Evolution of kinetic energies with time for a granular column collapse in fluid ($a = 4$)



(a) Normalised final run-out distance for columns with different initial aspect ratios. Comparison of dry and submerged granular column collapse.



(b) Normalised final collapse height for columns with different initial aspect ratios. Comparison of dry and submerged granular column collapse.

Figure 5.15 Normalised final collapse run-out and height for columns with different initial aspect ratios.

5.3.3 Effect of permeability

? observed development of large negative pore-pressure during dispersion of grains. The rate of dissipation of the negative pore-pressure is directly proportional to the permeability of the granular assembly. In the previous section, the evolution of run-out with the initial aspect ratio is studied using a constant hydrodynamic radius $r = 0.7 R$. In order to understand the effect of permeability on the run-out behaviour, the hydrodynamic radius r is varied from $0.7 R$ to $0.95 R$ for all aspect ratios. Increase in the hydrodynamic radius decreases the permeability of the granular assembly resulting in a longer duration for the dissipation of negative pore-pressure.

The normalised run-out for different hydrodynamic radii for a granular column with an initial aspect ratio of 0.8 are presented in figure 5.16. The run-out increases with decrease in the permeability, which is equivalent to an increase in the hydrodynamic radius. An increase in the hydrodynamic radius from 0.7 to 0.95 R increases the normalised run-out by 25%. However, even under a very low permeability condition ($r = 0.95 R$), the run-out observed in fluid is shorter than the dry and the buoyant conditions.

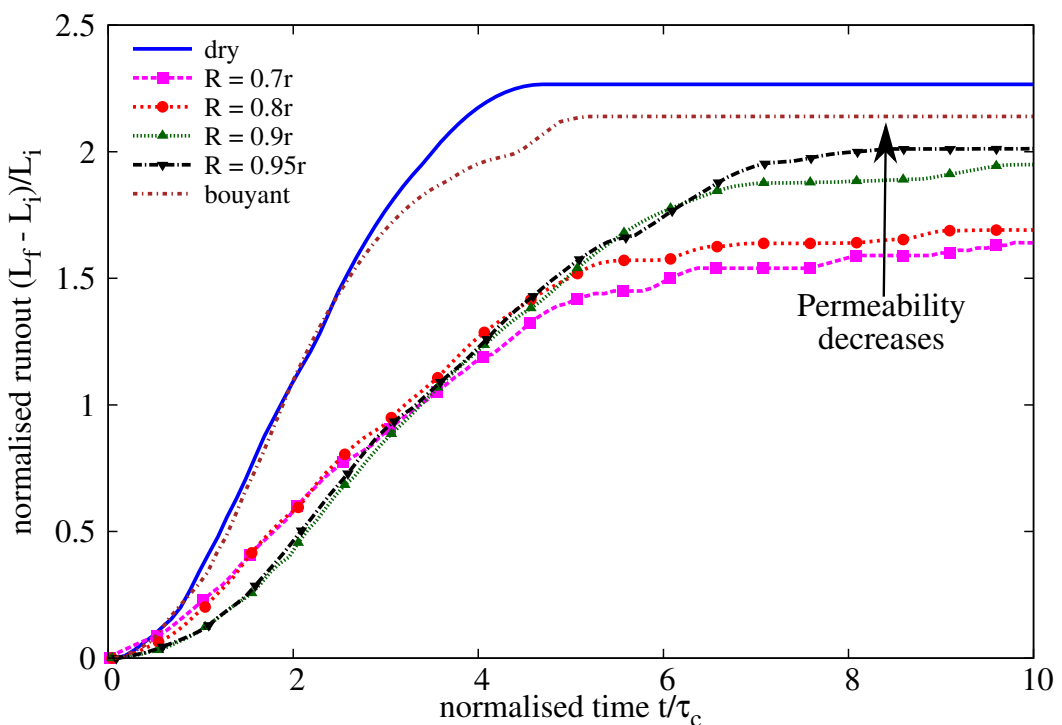


Figure 5.16 Effect of permeability on the evolution of run-out for a column collapse in fluid ($\alpha = 0.8$)

At a high permeability ($r = 0.7 R$), the evolution of run-out at the initial stage is quicker, which means that the negative pore-pressure that is developed during the shearing along the fracture surface is dissipated faster. Even though the negative pore-pressure is dissipated,

due to the development of negative pore-pressure the evolution of run-out in fluid is slower than its dry counterpart. The rate of dissipation decreases with decrease in the permeability. This can be observed by a flatter slope in the run-out evolution with decrease in permeability. Figure 5.17 shows the distribution of pore-pressure in high and low permeable granular media. At the same time $t = \tau_c$, the highly permeable ($r = 0.7 R$) granular column shows smaller negative pore-pressure in comparison to large negative pore-pressures observed in the shearing zone of a low permeable column ($r = 0.9 R$). This shows that not only does it take longer for the pore-pressure to dissipate with a decrease in permeability, but also results in almost twice the negative pore-pressure than what is observed in the high permeable case (figure 5.17b).

Although the low permeable granular columns require a longer duration for the run-out to evolve, the final run-out distance is found to be much longer than the high permeable condition. Figure 5.18 shows that the potential energy available for the flow of a low permeable column is 20% smaller than the collapse of a high permeable granular column. The kinetic energy evolution (figure 5.19) shows that the low permeable column has a wider peak kinetic energy distribution in comparison to a sharp peak observed in the high permeable condition. This indicates the influence of lubrication, i.e., hydroplaning of the granular flow in low permeable conditions. The evolution of the horizontal kinetic energy with time reveals that the peak kinetic energy is sustained longer as the permeability of the granular material decreases (figure 5.19b). Although, the peak kinetic energy is smaller in the low permeability case, the hydroplaning of the flowing granular mass results in a longer run-out distance. A high positive pore-pressure is observed at the base of the granular flow in low permeability condition (figure 5.20b) indicating the occurrence of hydroplaning. The evolution of local packing density shows a drop in the packing density at low permeability (figure 5.21). This drop in the value of packing density between $t = 2\tau_c$ and $t = 3\tau_c$ corroborates with the duration of hydroplaning during which a large amount of water is entrained at the flow front.

High permeable granular column shows lower water entrainment, which indicates that for highly permeable flows the drag force acting on the soil grains predominates over the lubrication effect on the run-out behaviour. In both the low and high permeable granular flows, the granular material consolidates at the final stage of the flow. This can be observed by the increase in the packing density at the final stage due to settlement of grains and expulsion of entrained water. The final deposit profile for both low and high permeability conditions are shown in figure 5.22. The high permeable collapse show a more parabolic (convex) deposit profile in contrast to the more concave profile observed in the low permeability condition. The observation of hydroplaning in the low permeable condition may be due to the difference in the distribution of granular mass at the flow front. Instigation of hydroplaning is controlled

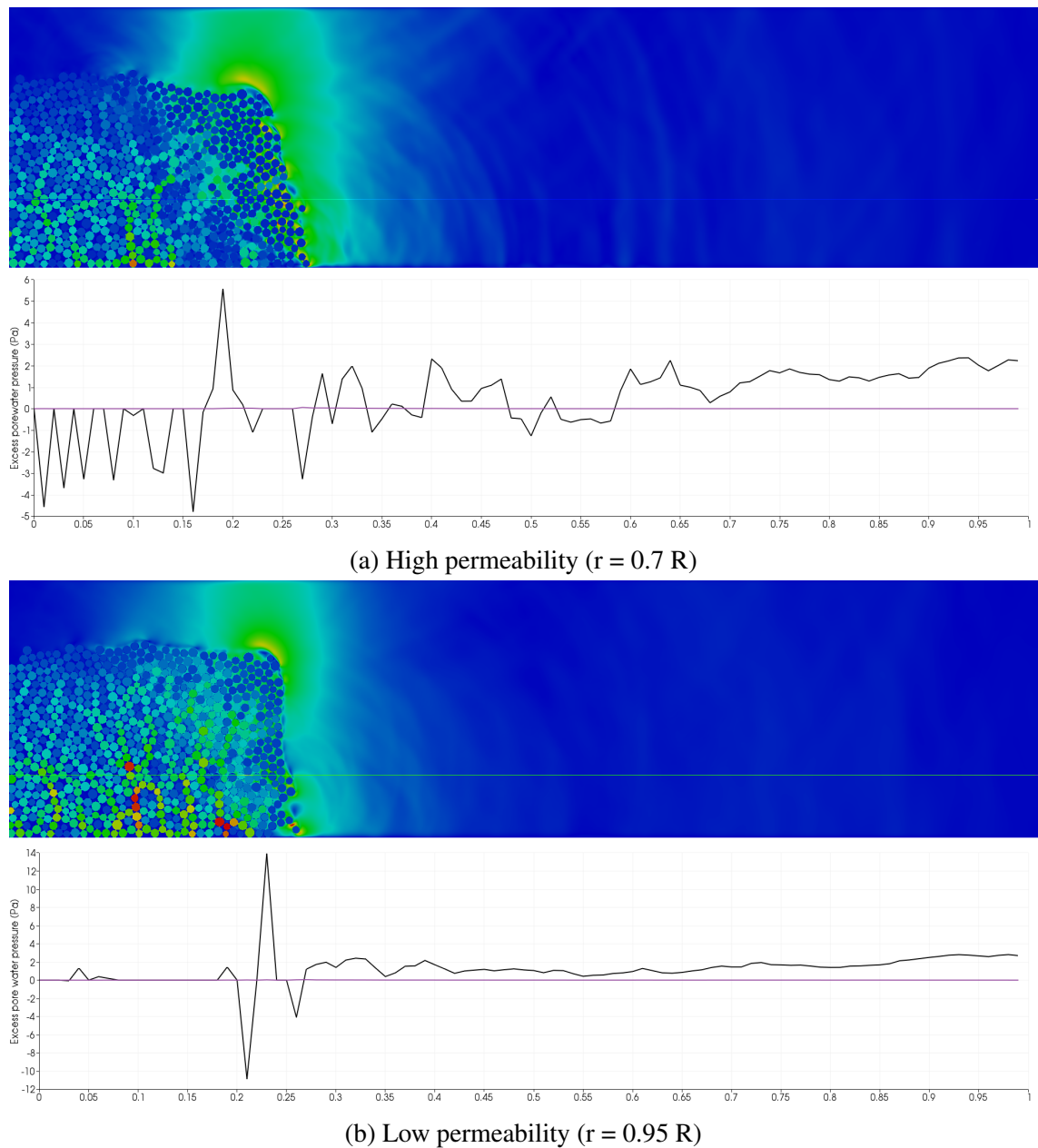


Figure 5.17 Effect of permeability on the excess pore water pressure distribution for a granular column collapse in fluid ($a = 0.8$ & dense packing) at $t = \tau_c$

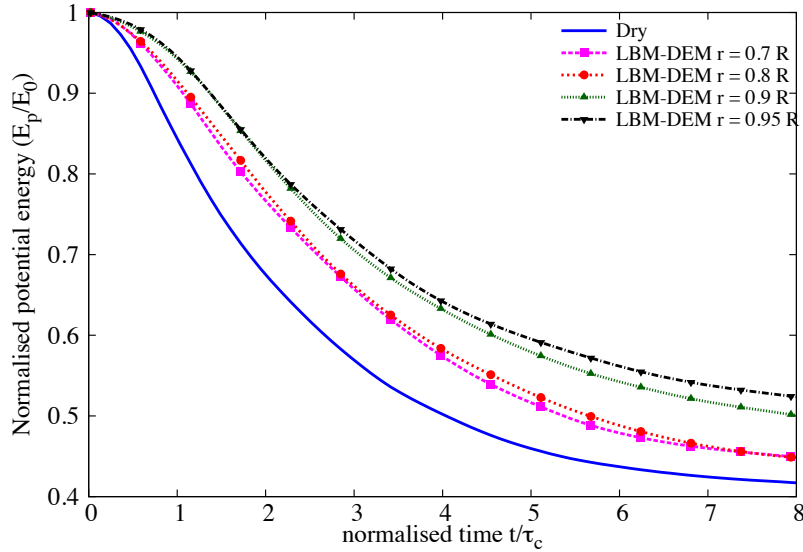


Figure 5.18 Effect of permeability on the evolution of the potential energy with time for a granular column collapse in fluid ($a = 0.8$)

by the balance of gravity and inertia forces at the debris front and is suitably characterized by the densimetric Froude's number:

$$Fr_d = \frac{U}{\sqrt{(\frac{\rho_d}{\rho_w} - 1)gH \cos \theta}} \quad (5.6)$$

where U is the average velocity of sliding mass, ρ_d and ρ_w are the densities of soil and water, respectively, H is the thickness of the sliding mass, g is acceleration due to gravity and θ represents the slope angle. ? observed hydroplaning above a critical value of densimetric Froude's number of 0.4. A Froude's Fr_d value of 0.427 is observed for the low permeable flow ($r = 0.95 R$), which indicates the occurrence of hydroplaning. Whereas, a $Fr_d = 0.273$ is observed for the high permeable granular flow indicating absence of hydroplaning, the low permeable collapse is predominated by the viscous drag force resulting in a parabolic profile and shorter run-out distance.

The normalised final run-out distance as a function of the initial aspect ratio of the column is presented in figure 5.23. For all aspect ratios, the dry condition yields the longest run-out distance. For a given aspect ratio, the dry collapse acquires the highest peak kinetic energy due to the lack of viscous dissipation during vertical collapse. This extra kinetic energy is high enough to propel the heap, in spite of a high frictional dissipation, over a distance that is longer than the run-out distance in the fluid regime. In the submerged condition, for the

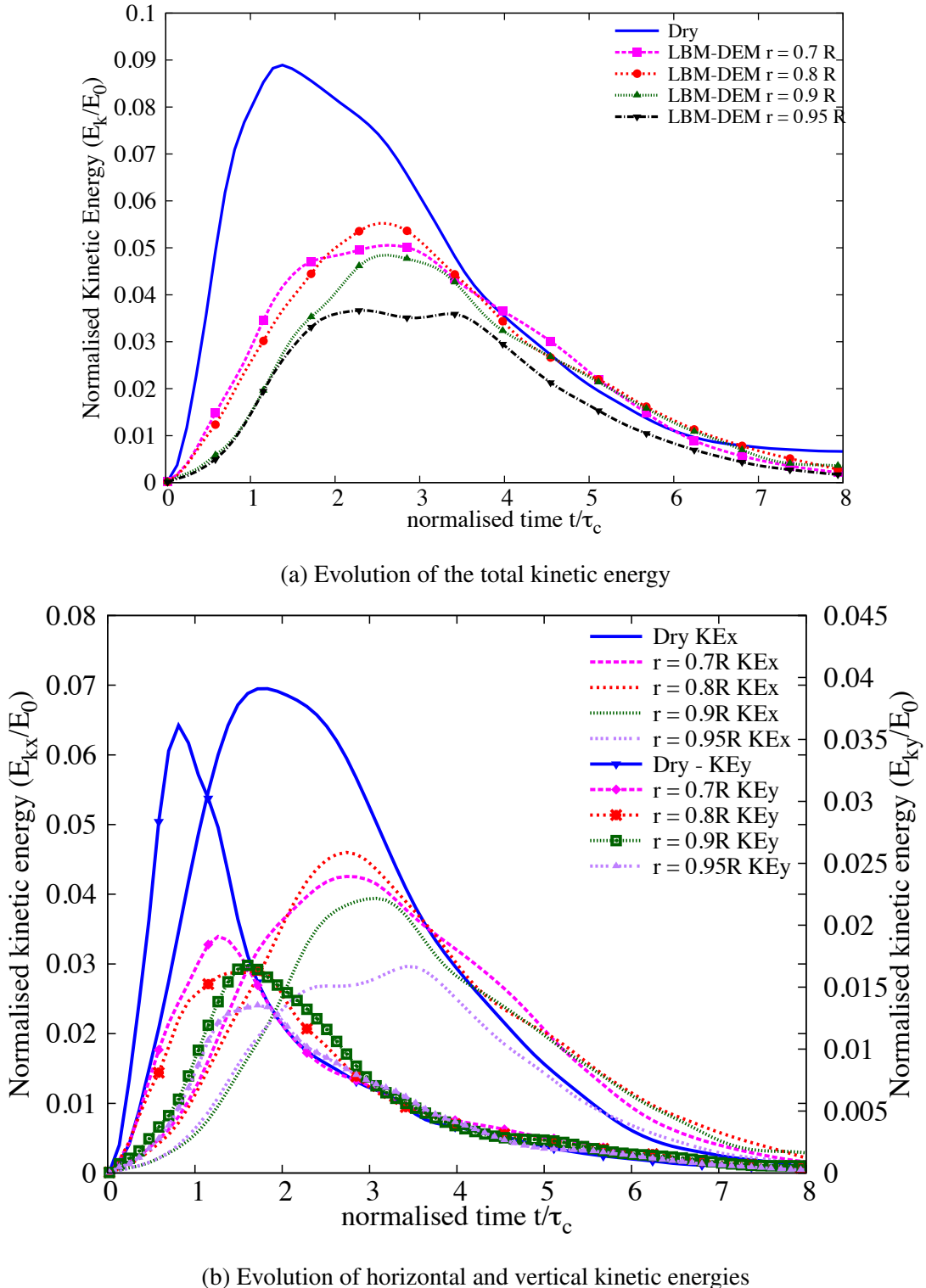


Figure 5.19 Effect of permeability on the evolution of kinetic energies with time for a granular column collapse in fluid ($a = 0.8$)

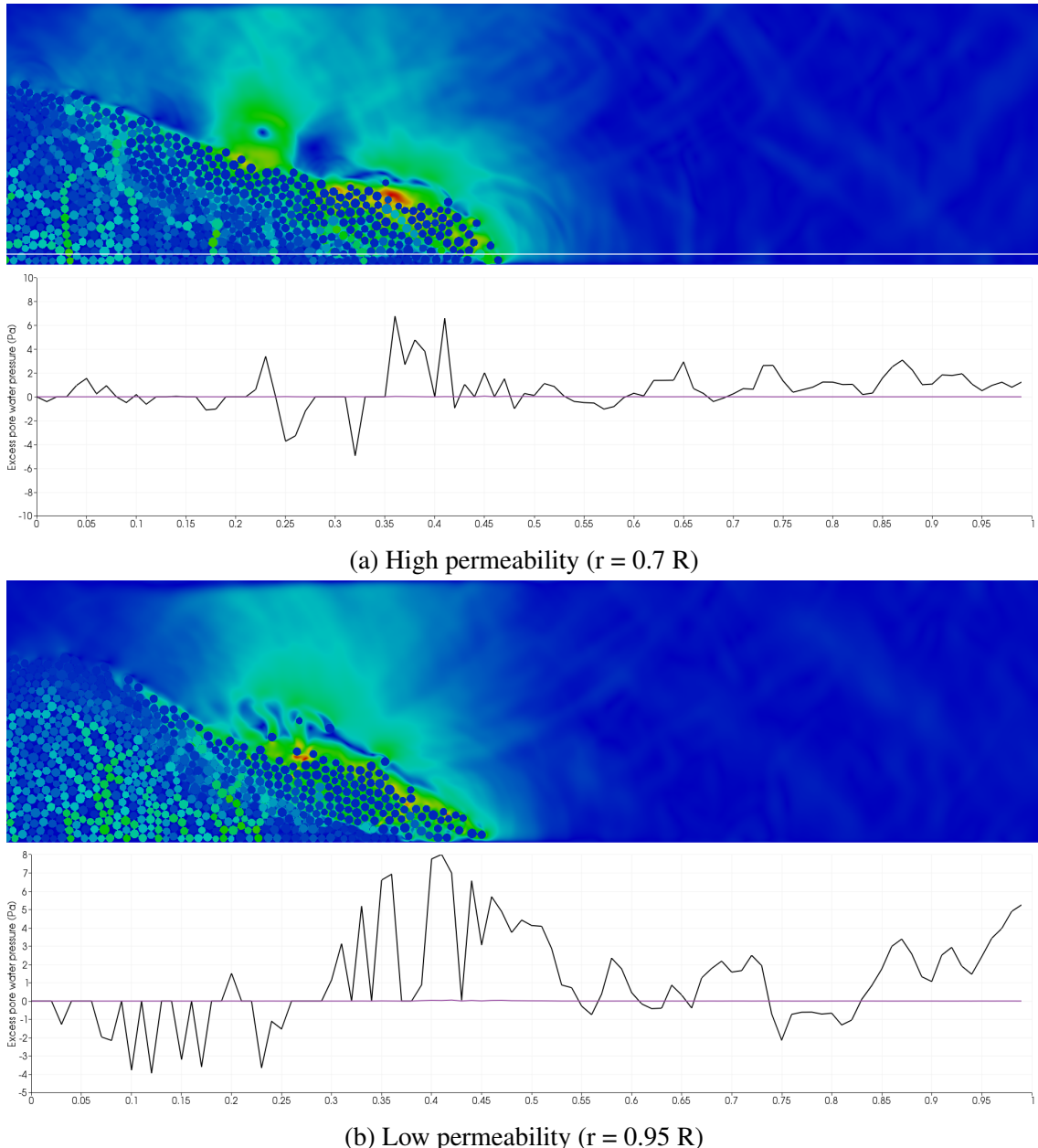


Figure 5.20 Effect of permeability on the excess pore water pressure distribution for a granular column collapse in fluid ($a = 0.8$ & dense packing) at $t = 2\tau_c$

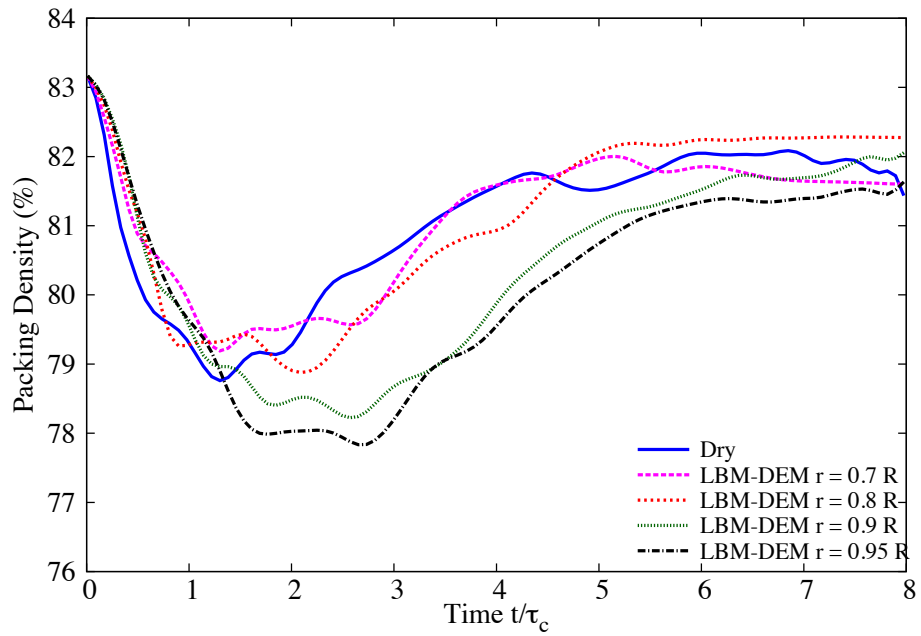
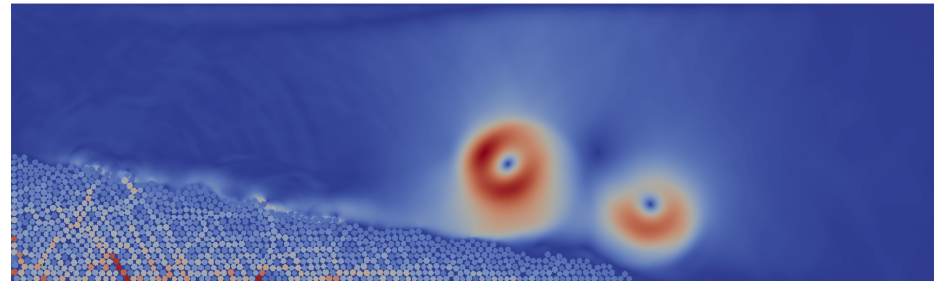
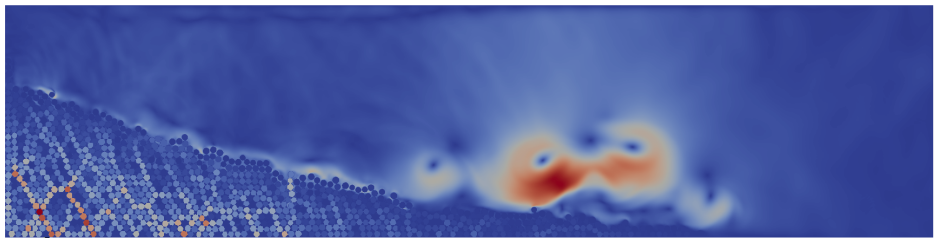


Figure 5.21 Effect of permeability on the evolution of packing density for a granular column collapse in fluid ($a = 0.8$ & dense initial packing)



(a) High permeability ($r = 0.7 R$)



(b) Low permeability ($r = 0.95 R$)

Figure 5.22 Effect of permeability on the deposit morphology of a granular column collapse in fluid ($a = 0.8$)

same aspect ratio, the kinetic energy available for spreading is lower and the dissipation due to viscous drag is higher, thus leading to a much shorter run-out distance.

For short columns, with decrease in permeability the run-out distance increases, however, the run-out distance is not higher than the dry condition. At higher aspect ratios, decrease in permeability from $r = 0.8 R$ to $r = 0.9 R$ does not have a significant influence on the run-out behaviour. This can be attributed to the turbulent nature of the granular flows for tall columns. The run-out behaviour is a result of transformation of (part of) the initial potential energy to the peak kinetic energy, which in turn controls the subsequent run-out along the plane. The run-out distance is plotted as a function of the normalised peak kinetic energy in figure 5.24. For the same aspect ratio, the peak kinetic energy is higher in the case of dry column. This represents grain inertial regime in dry granular collapse, which indicates that a part of the potential energy, in the presence of the fluid, is dissipated during the vertical collapse due to viscous friction. In all regimes, the run-out distance increases as a power law $L_f \propto KE_{max}^\gamma$. For the same value of peak kinetic energy, the run-out distance in fluid is longer than the dry column collapse. Also, with decrease in permeability the run-out distance increases for the same peak kinetic energy.

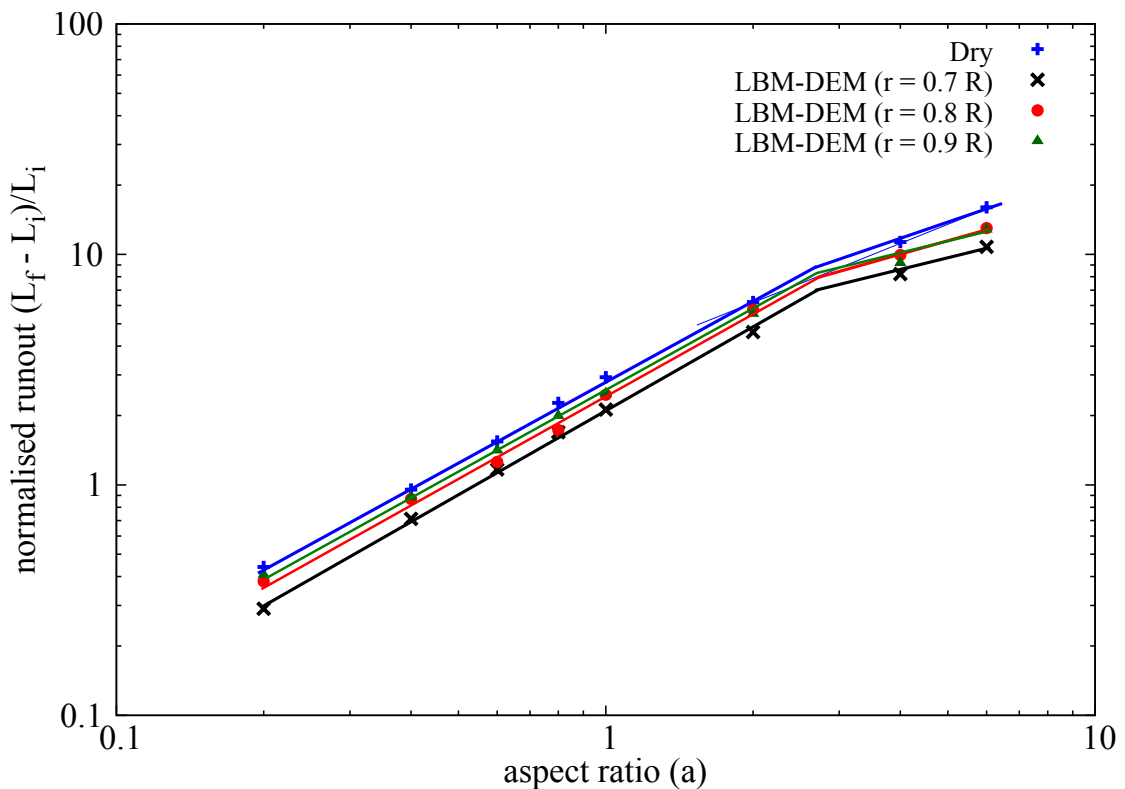


Figure 5.23 Normalised final run-out distance for columns with different initial aspect ratios. Comparison of dry and submerged granular column collapse for different hydrodynamic radius (0.7 R, 0.8 R and 0.9 R).

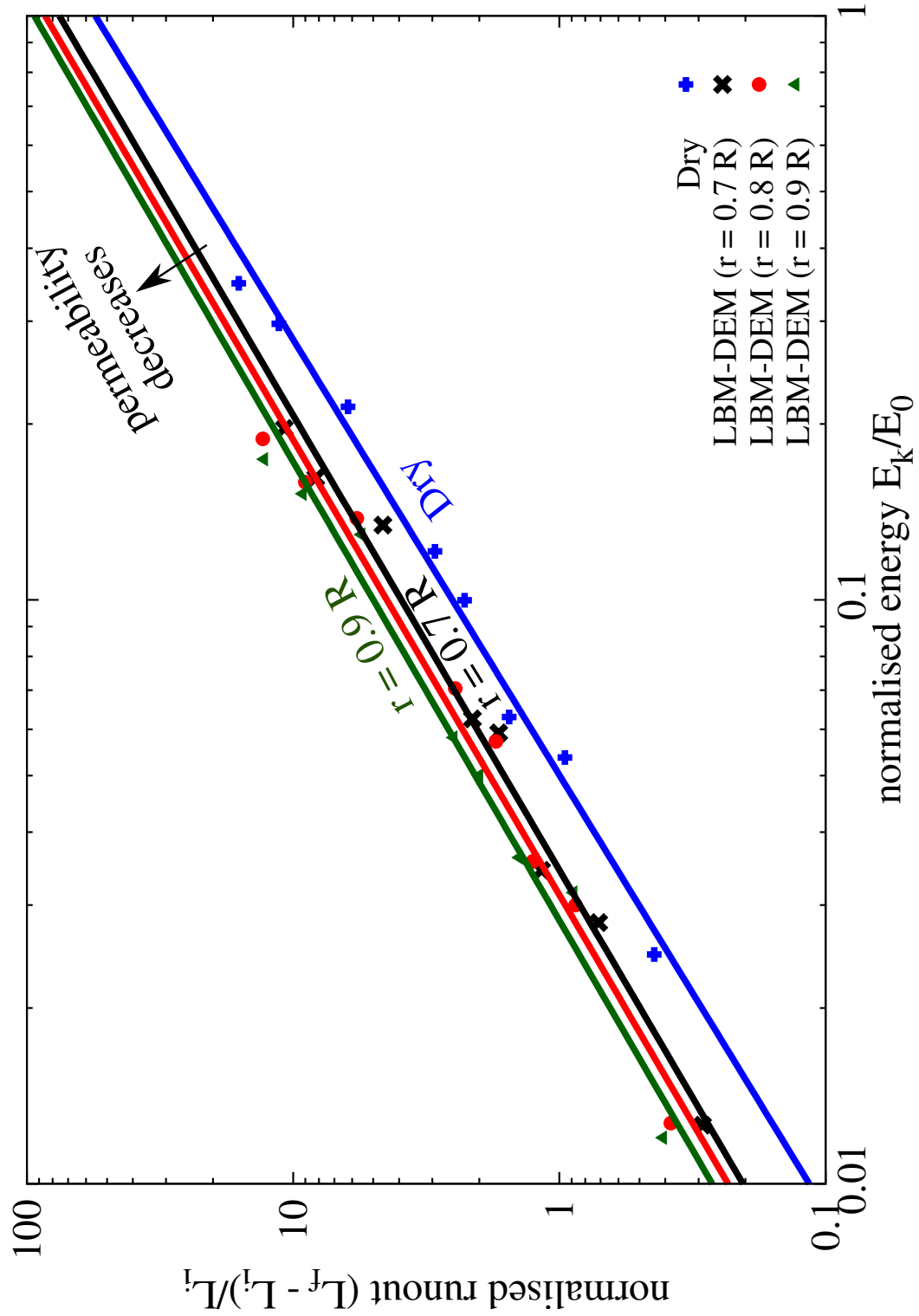


Figure 5.24 Normalised final run-out distance for columns as a function of peak kinetic energy. Comparison of dry and submerged granular column collapse for different hydrodynamic radius (0.7 R, 0.8 R and 0.9 R).

5.3.4 Effect of initial packing density

Rondon et al. (2011) observed that the loose packings flow rapidly on a time scale proportional to the initial height and results in longer run-out distance in comparison to the dense packing. Hydroplaning occurs above a critical Froude's number of 0.4. The Froude's number is inversely related to the thickness of the flow and its density. Hence, for the same thickness of flow, a loose granular column will experience more hydroplaning than a dense granular flow. This effect might result in longer run-out behaviour in fluid than the dry condition for the same initial aspect ratio. The initial packing density and the permeability of a 2D granular column, with an aspect ratio of 0.8, are varied to understand their influence on the run-out behaviour. The run-out behaviour of the dense case (83% packing density), discussed in the previous section, is compared with a loose granular column (79% packing fraction). The permeability is varied by changing the hydrodynamic radius from 0.7 R to 0.95 R.

The normalised run-out evolution with time for a loose initial packing (79% packing fraction) with different hydrodynamic radii 0.7 R, 0.8 R, 0.9 and 0.95 R are presented in figure 5.25. The run-out evolution of dry and a column with grains in suspension with an initial aspect ratio of 0.8 are also presented to understand the influence of hydrodynamic forces on the flow kinematics. Similar to the dense granular column, the run-out distance increases with increase in the hydrodynamic radius (i.e., decrease in permeability). At low permeabilities ($r = 0.9$ and 0.95 R), the run-out distance is longer than the dry condition. This shows that the lubrication effect in low permeability condition overcomes the influence of the drag force and the development of large negative pore-pressure resulting in a longer run-out distance. Although suspended granular masses experience high drag force and turbulent effects, the run-out evolves almost at the same rate in comparison with granular columns with high permeability. This shows the effect of permeability on the dissipation rate of negative pore-pressure developed during the initial stage of collapse.

Figure 5.26 shows the development of negative pore-pressure in low permeability ($r = 0.95$ R) and dissipation of negative pore-pressure in high permeability ($r = 0.7$ R) at the same time $t = \tau_c$. This difference in the quantity and the rate of dissipation of negative pore-pressure results in a difference in the rate of flow evolution. A low permeable column requires a longer duration to evolve. As the flow progresses, the low permeability of the granular column causes hydroplaning to occur at the base of the column resulting in longer run-out distance (figure 5.27).

The evolution of the potential energy with time reveals that at a very low permeability ($r = 0.95$ R), the initial potential energy mobilised is smaller than at $r = 0.9$ R. Also with decrease in permeability, the time required to dissipate the negative pore-pressure increases. This results in a shorter run-out distance in the case of $r = 0.95$ R to that of $r = 0.9$ R. As the

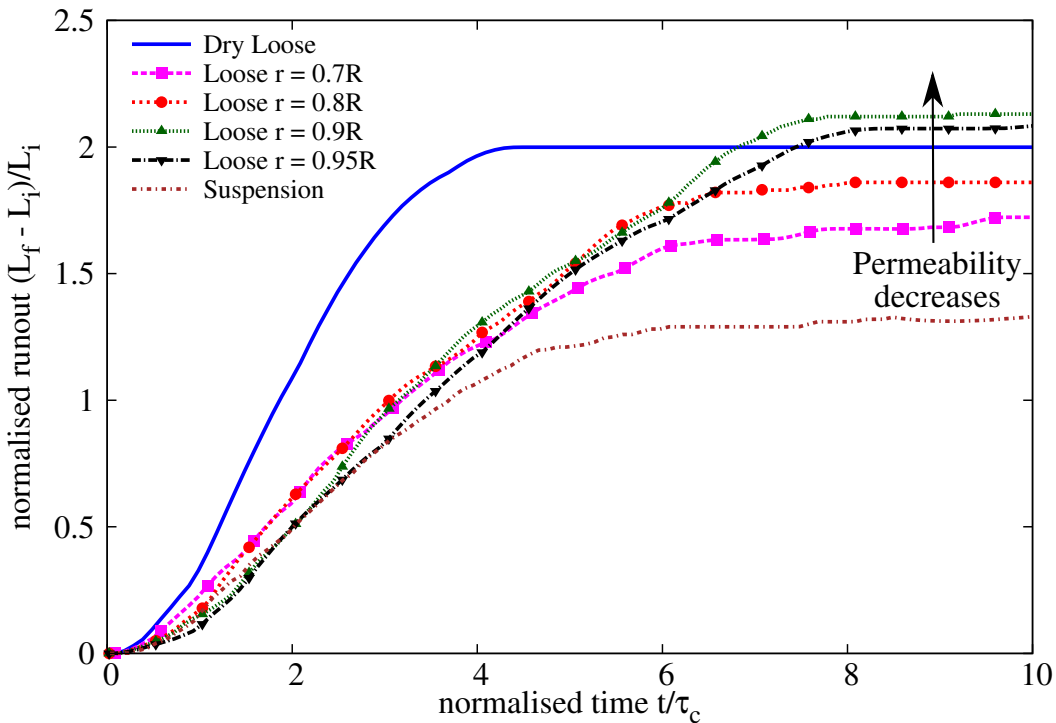


Figure 5.25 Effect of permeability on the evolution of run-out for a column collapse in fluid ($a = 0.8$ & loose packing)

quantity of material destabilised is small, the flow is thinner and thus has a high Froude's number. However, the peak horizontal kinetic velocity observed in the case of $r = 0.9$ R is higher than $r = 0.95$ R (figure 5.30b). A Froude's number of 0.59 for $r = 0.9$ R is observed in contrast to 0.46 for $r = 0.95$ R. Both values of hydrodynamic radii result in a Froude's number that indicates occurrence of hydroplaning. However, the difference in the amount of material destabilised for $r = 0.95$ R and the decreased effect of hydroplaning results in a shorter run-out distance for $r = 0.95$ R in comparison to $r = 0.9$ R.

As the column collapses, water is entrained at the flow front. This can be observed by the decrease in the packing fraction during $t = 1\tau_c$ and $t = 3\tau_c$. As the flow progresses, the entrained water is expelled and the soil grains consolidate to reach a critical packing density at the end of the flow (figure 5.29). The permeability (hydrodynamic radius) plays a crucial role in the rate of dissipation of the entrained water. As the permeability decreases, the water entrained at the flow front takes longer time to be dissipated resulting in lubrication of the flow at low permeabilities. This lubrication effect results in an increase in the run-out distance for columns with low permeabilities.

The evolution of grain trajectories with time are presented in figure 5.31 for low ($r = 0.95$ R) and high ($r = 0.9$ R) permeability conditions. It can be observed that a high permeability

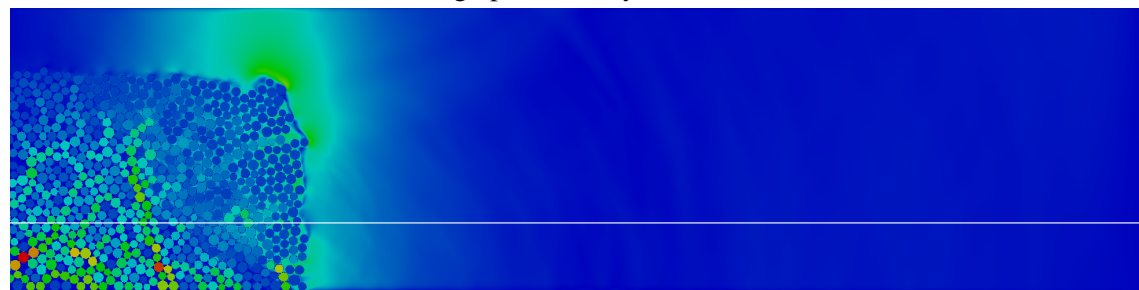
(a) High permeability ($r = 0.7 R$)(b) Low permeability ($r = 0.95 R$)

Figure 5.26 Effect of permeability on the excess pore water pressure distribution for a granular column collapse in fluid ($a = 0.8$ & loose packing) at $t = \tau_c$

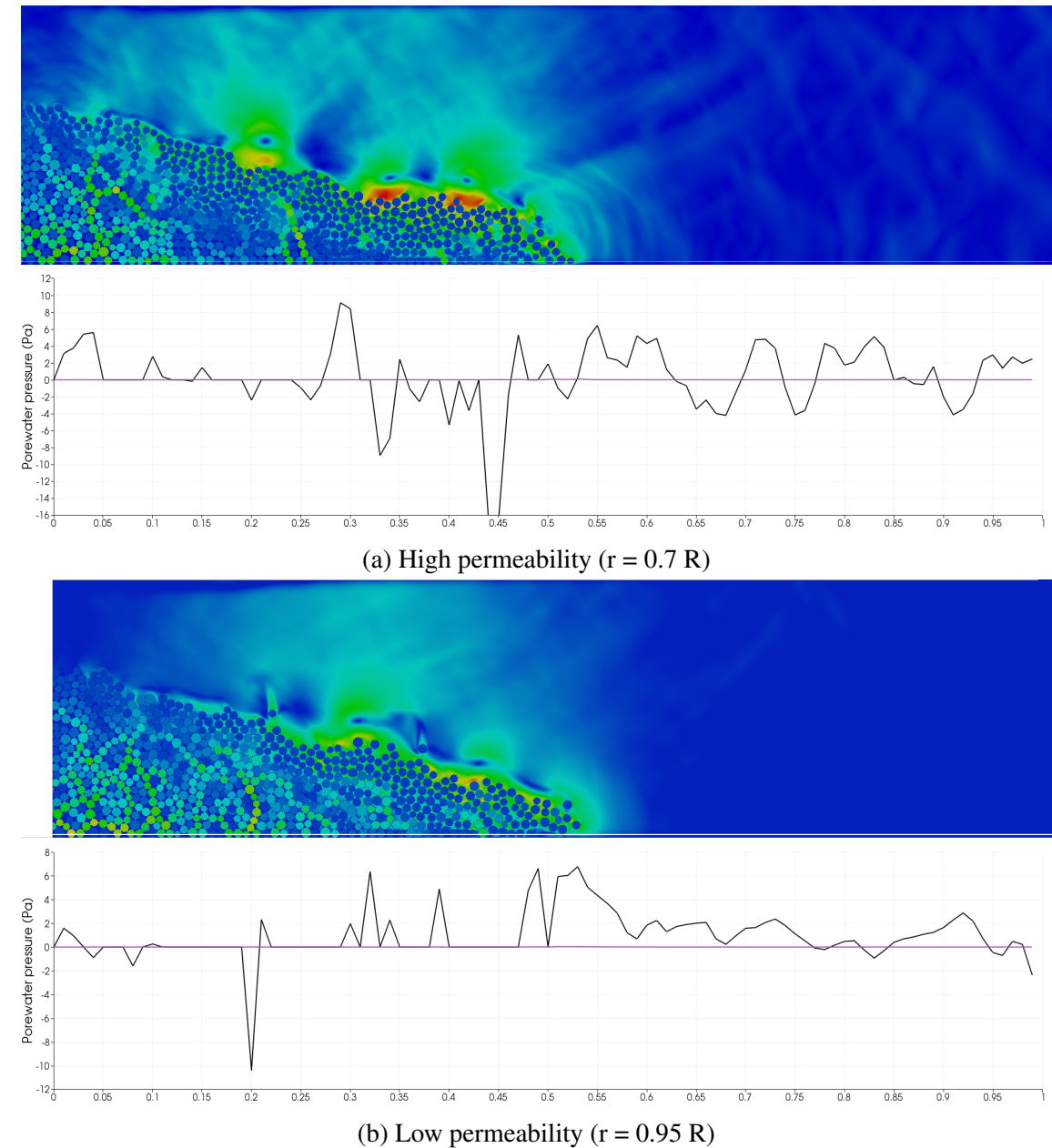


Figure 5.27 Effect of permeability on the excess pore water pressure distribution for a granular column collapse in fluid ($a = 0.8$ & loose packing) at $t = 2\tau_c$

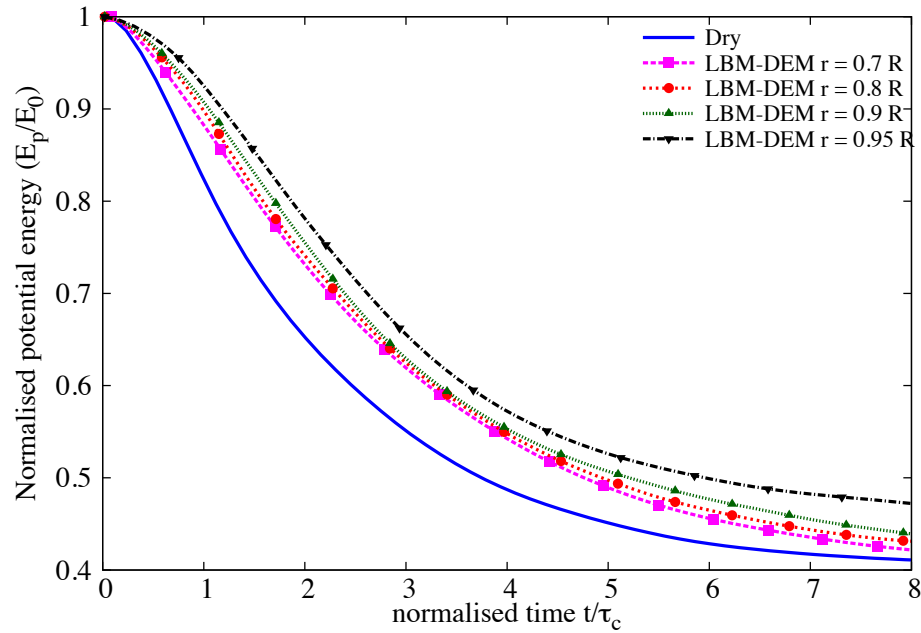


Figure 5.28 Effect of permeability on the evolution of the potential energy with time for a granular column collapse in fluid ($a = 0.8$ & loose packing)

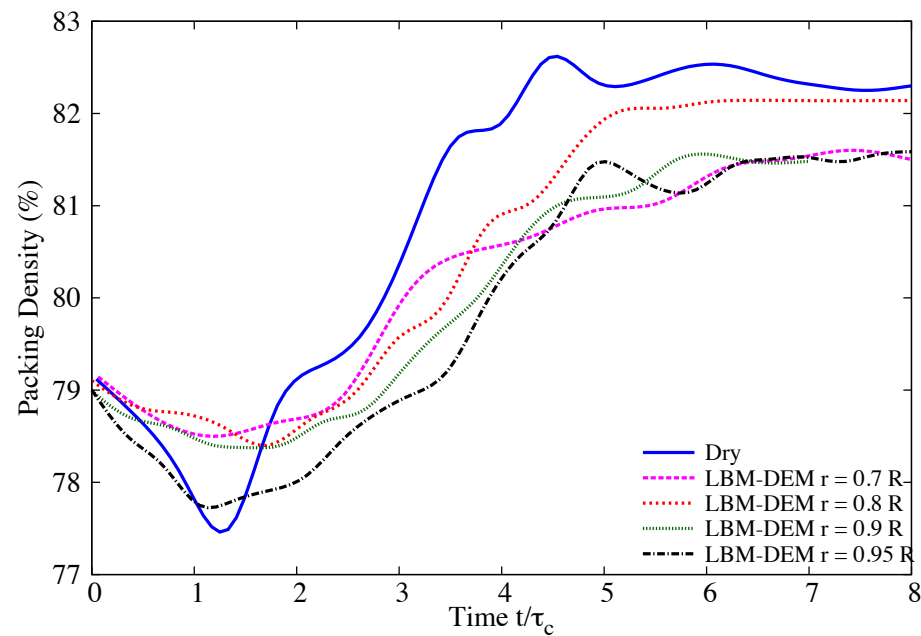


Figure 5.29 Effect of permeability on the evolution of packing density for a granular column collapse in fluid ($a = 0.8$ & loose initial packing)

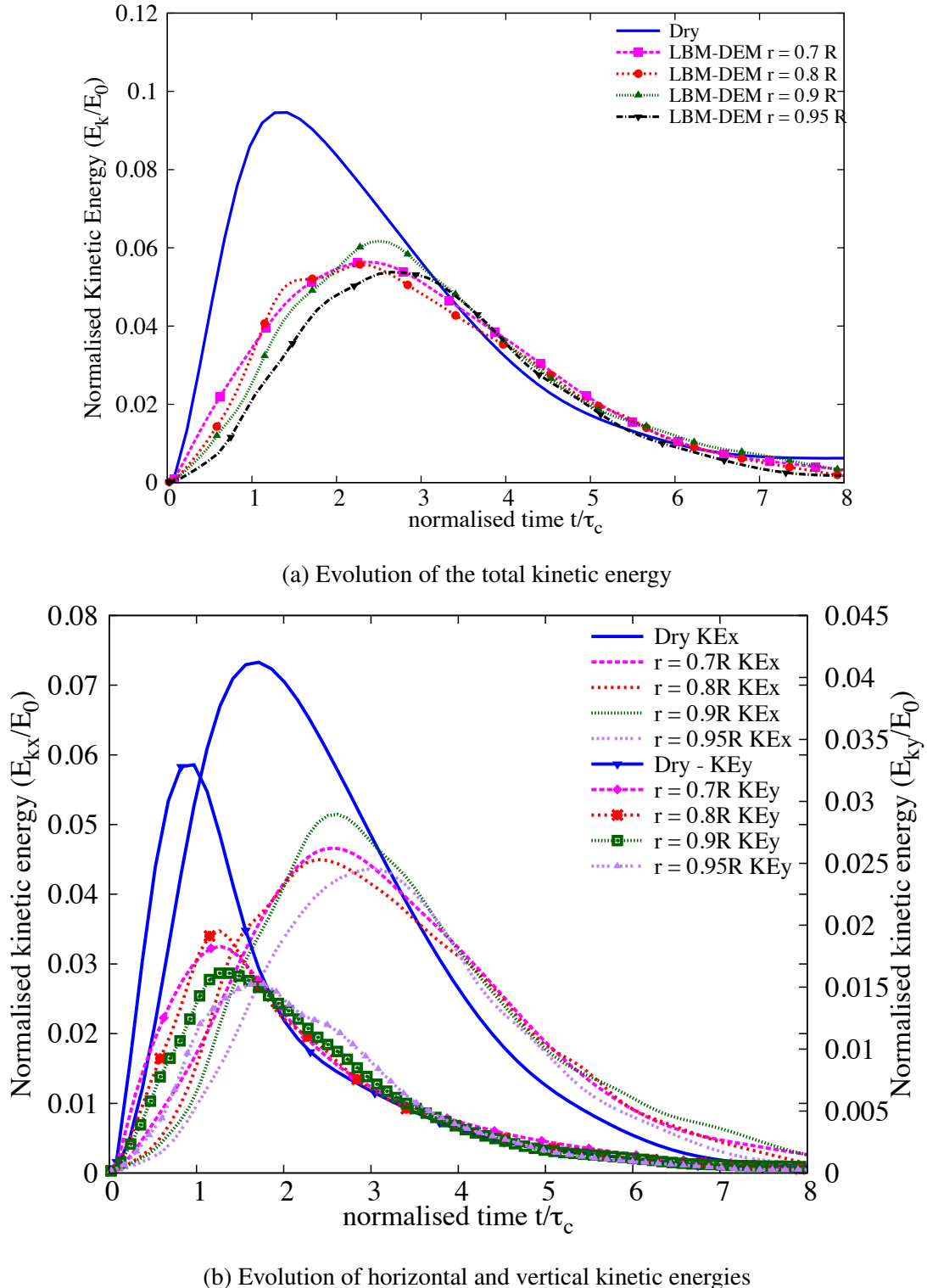


Figure 5.30 Effect of permeability on the evolution of kinetic energies with time for a granular column collapse in fluid ($a = 0.8$ & loose packing)

column shows a parabolic (convex) final profile in contrast to the more concave profile observed in low permeability condition. This difference in the flow thickness results in a higher value of Froude's number and the occurrence of hydroplaning in the low permeability condition. Due to the high permeability, the water entrained at the flow front is dissipated quicker and thus no lubrication effect is observed. A Froude's number of 0.272 (no hydroplaning) is observed for the high permeability condition ($r = 0.7 R$). This shows that the drag force predominates at high permeability, while the low permeability condition is characterised by hydroplaning and lubrication.

Figure 5.32 shows the normalised pressure at the base for the low and high permeability flows at $t = 2\tau_c$. The normalised effective stress plotted is obtained as the average over 5 time steps at $2\tau_c$. The effective stress at the base is normalised to the effective stress of a static granular column before the collapse. A value of 1 indicates that the effective stress hasn't changed, which can be observed in the static region of the granular column. It can be observed that the normalised effective stress is significantly higher for the high permeability condition at the flow front in comparison to the almost non-existence of effective stress in the low permeability condition. The observation of trivial effective stress at the flow front corroborates the lubrication effect observed at low permeability conditions.

Figure 5.33 shows the grain trajectories of a dense and a loose initial packing for a hydrodynamic radius ($r = 0.95 R$). It can be observed that the dense initial packing results in a lot of turbulent behaviour at the flow surface in contrast to the more plug like flow observed in the loose condition. The thickness of the deposit in both dense and loose condition is almost the same, however the density of the flow results in a Froude's number of 0.46 and 0.429 for loose and dense conditions, respectively. The low initial density results in more hydroplaning in the loose condition. The effect of water entrainment at the flow front between dense and loose condition can be seen in figure 5.34. Comparing the packing density (figures 5.21 and 5.29) reveals almost the same amount of water entrainment in both dense and loose conditions. Hence, it is the density of the flowing granular mass that controls the influence of hydroplaning for a given hydrodynamic radius and initial aspect ratio. A loosely packed granular column with low permeability entrains more water at the flow front, resulting in a hydroplaning effect that overcomes the influence of viscous drag forces and thereby yields a higher run-out distance than the dry condition.

Rondon et al. (2011) also observed that the collapse of a granular column in a viscous fluid is mainly controlled by the initial volume fraction and not by the aspect ratio of the column. The role of the initial volume fraction observed explains the pore pressure feedback mechanism proposed by (??) in the context of landslides. The compaction or dilation of grains can cause additional stress in the grains which can stabilise or destabilise the soil. The

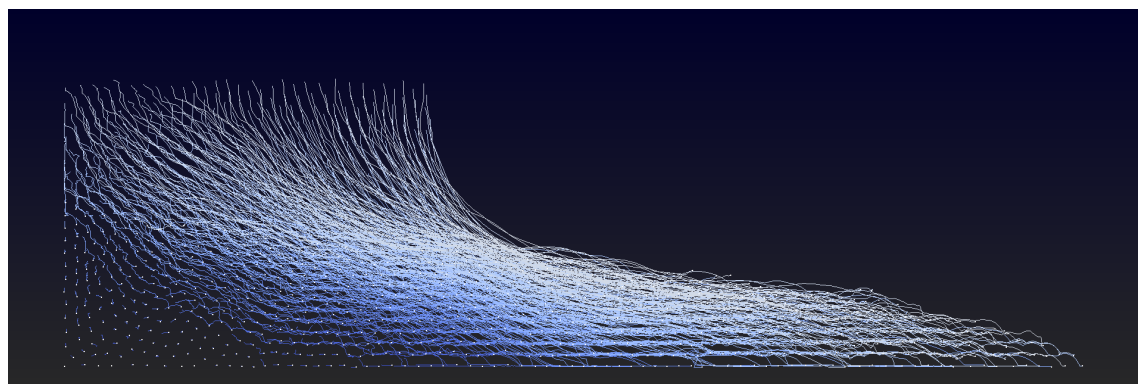
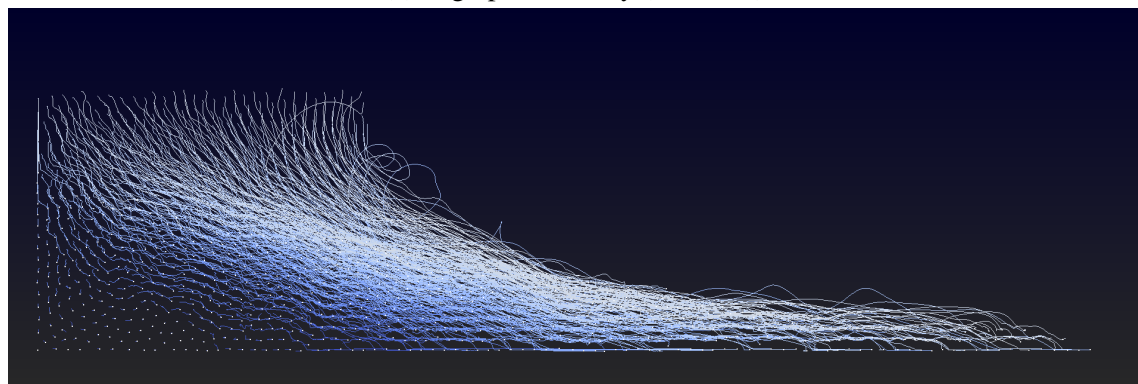
(a) High permeability ($r = 0.7 R$)(b) Low permeability ($r = 0.95 R$)

Figure 5.31 Particle tracking of the deposit morphology for a granular column collapse in fluid ($a = 0.8$ & loose packing), influence of permeability

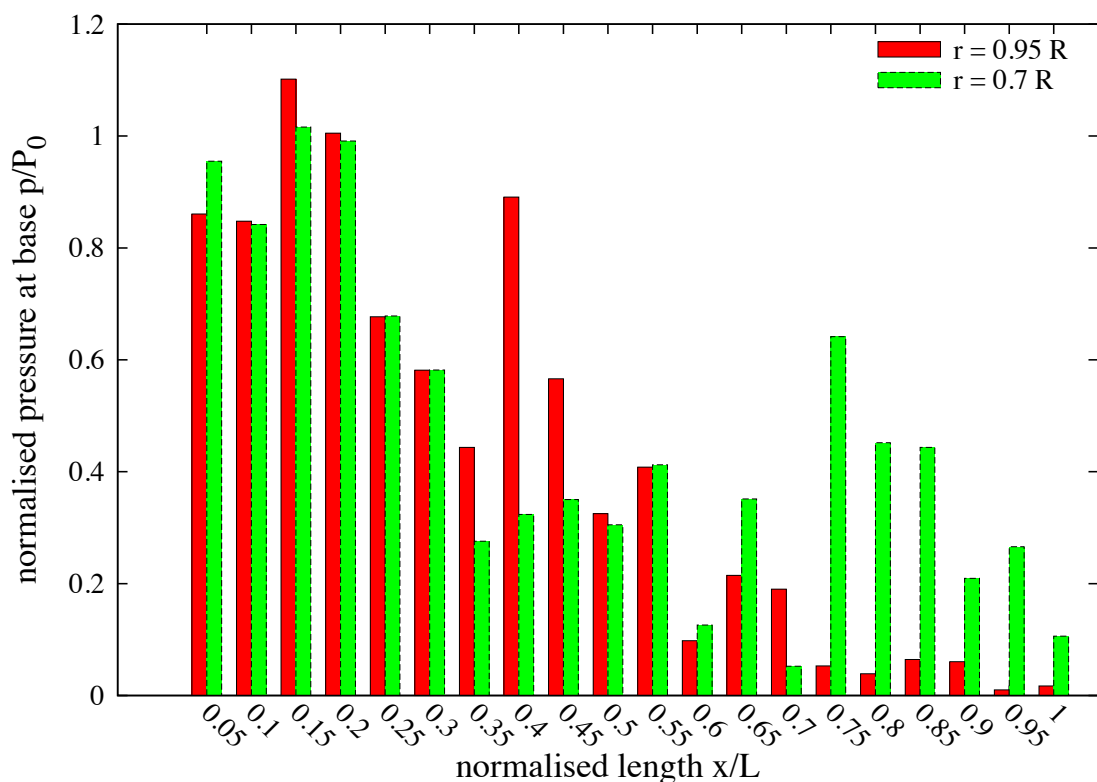


Figure 5.32 Effect of permeability on the normalised effective stress for loose initial packing at $t = 2\tau_c$

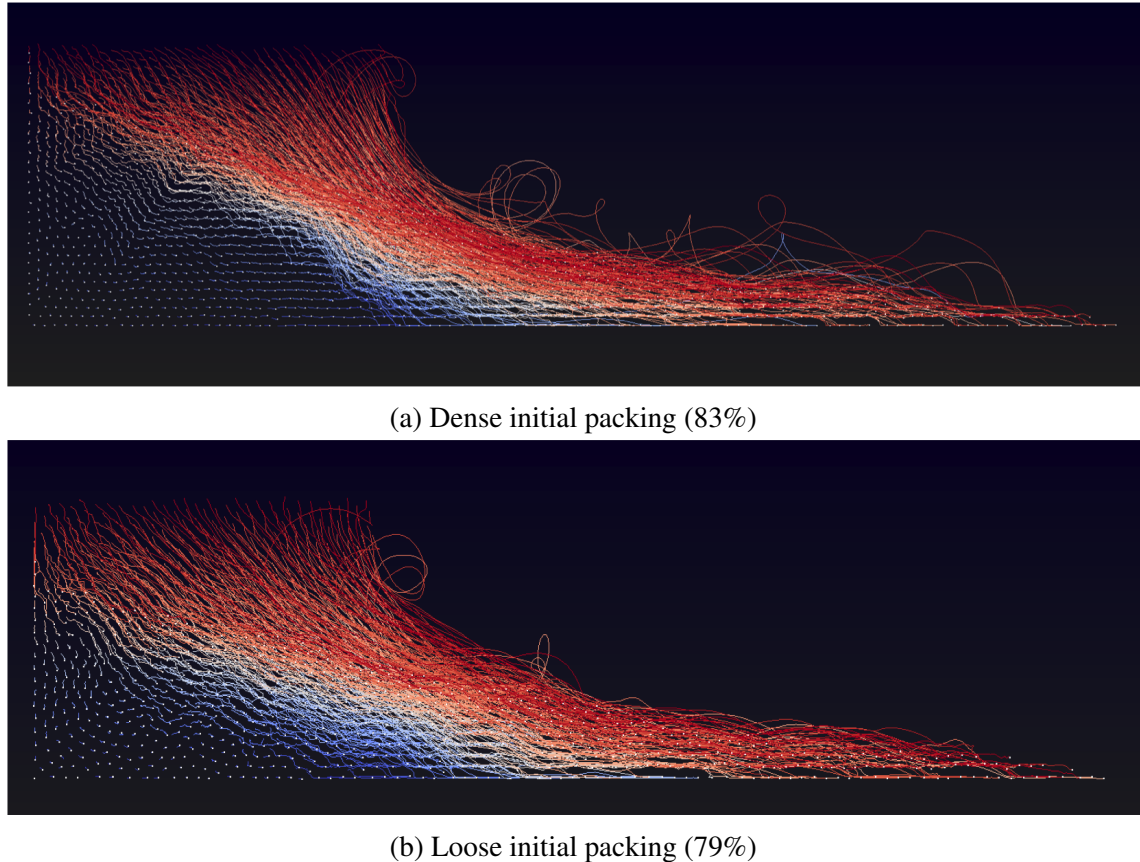
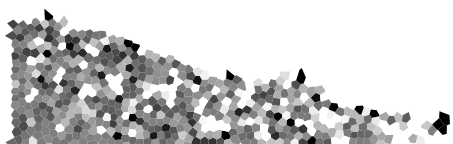


Figure 5.33 Effect of initial density on the deposit morphology for a granular column collapse in fluid ($a = 0.8$). Dense vs loose initial packing fraction ($r = 0.95 R$). Darker means dense packing, white indicates loose packing density.

flow is thus controlled by the coupling between the dilatancy of the granular layer and the development of pore pressure in the fluid phase (?). The dense column needs to dilate in order to flow. When it starts to fall, liquid is then sucked into the column, which is then stabilized by the additional viscous drag (Rondon et al., 2011; Topin et al., 2012). By opposition the loose column when it starts flowing expands and ejects liquid, leading to a partial fluidisation of the material.



(a) Dense initial packing (83%)



(b) Loose initial packing (79%)

Figure 5.34 Evolution of packing fraction at $t = \tau_c$ for dense and loose initial packing fraction.

5.4 Submarine granular flows down incline plane

Slope failure is a problem of high practical importance for both civil engineering structures and natural hazards management. Catastrophic events such as landslides, debris flows, rock avalanches or reservoir embankment failures exemplify the potential consequences of a soil gravitational instability. One of the most critical situations concerns a submerged sandy slope as pore pressure changes, seepage or earthquakes can cause significant damages to off-shore structures and may generate a tsunami.

The influence of slope angle on the effect of permeability and the initial packing density on the run-out behaviour are studied. In this study, a 2D poly-disperse system ($d_{max}/d_{min} = 2$) of circular discs forming a granular column in fluid is used to understand the behaviour of granular flows down inclined planes (Figure 5.5). The soil column is modelled using ~ 1000 to 2000 discs of density 2650 kg m^{-3} and a contact friction angle of 26° . The collapse of the granular column is simulated inside a fluid with a density of 1000 kg m^{-3} and a kinematic viscosity of $1 \times 10^{-6} \text{ m}^2 \text{ s}^{-1}$. A granular column with an initial aspect ratio α of 0.8 is used. A hydrodynamic radius $r = 0.9 R$ is adopted during the LBM computations. Dry analyses are also performed to study the effect of hydrodynamic forces on the run-out distance. The numerical configuration used in this study is shown in figure 5.5a. The slope angle θ is varied as 0° , 2.5° , 5° , and 7.5° . The effect of initial packing density is studied using a dense packing (83% packing fraction) and a loose packing (79% packing fraction) of granular columns that collapse on to an inclined plane at different slope angles. The influence of permeability (with hydrodynamic radius varied as 0.7 , 0.75 , 0.8 , 0.85 and $0.9 R$) on the run-out behaviour of collapse of granular columns with initial packing density of 83% and 79 % on to an inclined plane with a slope angle of 5° is also analysed.

5.4.1 Effect of initial density

The morphology of granular deposits in fluid is shown to be mainly controlled by the initial volume fraction of the granular mass and not by the aspect ratio of the column (Rondon et al., 2011; ?). In order to understand the influence of the initial packing density on the run-out behaviour, a dense sand column (initial packing density, $\Phi = 83\%$) and a loose sand column ($\Phi = 79\%$) are considered. The granular columns collapse and flow down slopes of varying inclinations (2.5° , 5° and 7.5°). The run-out behaviour is compared with the collapse of a granular column in fluid on a horizontal surface. For all slope angles, the flow kinematics in the submerged condition is compared with its dry counterpart to understand the influence of lubrication and viscous drag. A hydrodynamic radius of $r = 0.9 R$ is adopted in all cases,

because low permeability conditions result in longer run-out distance as observed in the previous section.

The evolution of run-out for a dense sand column with time in dry and submerged conditions for varying slope inclinations are presented in figure 5.35a. For all slope angles, the run-out distances in the dry condition are longer than those observed in the submerged condition. Similar to the case of collapse on a horizontal plane, the dense granular columns experience drag forces that have a significant influence than the lubrication effect. The difference in the run-out between the dry and the submerged condition decreases with increase in the slope angle. At a slope angle of 5° the difference in the run-out between the dry and the submerged condition is the smallest. This is due to significant hydroplaning of a thin flowing layer, the occurrence of hydroplaning can be observed by a sustained peak kinetic energy (figure 5.35b). At higher slope angles ($> 5^\circ$), the drag force predominates over the lubrication effect and results in shorter run-out distance.

Similar to the case of collapse on a horizontal surface, the dense granular columns in fluid require a longer time to collapse and flow, due to the development of large negative pore-pressure. Large negative pore-pressure are developed as the dense granular material dilates due to shearing along the fracture surface in the initial phase of the flow. The snapshots of the dense granular column collapse down slopes of varying inclinations at the time ($t = \tau_c = 3\sqrt{H/g}$), are shown in figure 5.36.

It can be seen that the viscous drag on the dense column tends to predominate over the influence of hydroplaning on the run-out behaviour. This influence can be observed in the smaller peak kinetic energy for submerged granular in comparison to the dry condition (Figure 5.35b). With increase in the slope angle, the volume of material that dilates increases. This results in large negative pore-pressure and more viscous drag on the granular material. Hence, the difference in the run-out between the dry and the submerged conditions, for a dense granular assembly, increases with increase in the slope angle above an inclination of 5° .

In contrast to the dense granular columns, the loose granular columns (packing fraction of 79%) show longer run-out distance in immersed conditions (Figure 5.37a). The run-out distance in fluid increases with increase in the slope angle in comparison to the dry cases. The loose granular flow tends to entrain more water at the base of the flow front, creating a lubricating surface, which results in a longer run-out distance (Figure 5.38). For the same thickness of the flow, the loose granular flow has smaller density and hence a higher Froude's number than the dense flow resulting in a higher probability of hydroplaning. The hydroplaning effect causes an increase in the flow velocity for the loose granular material in comparison with the dense condition (Figure 5.37b).

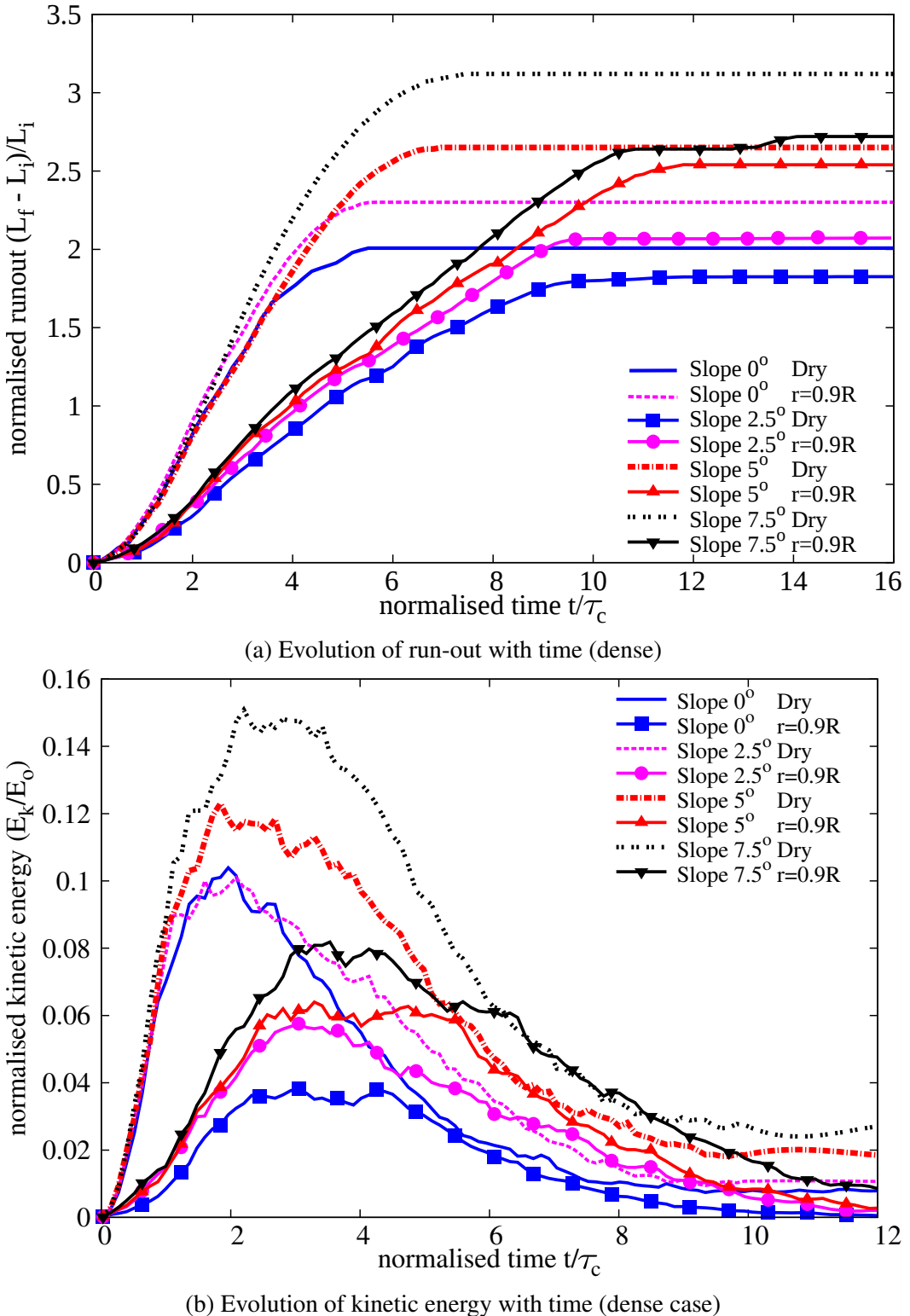
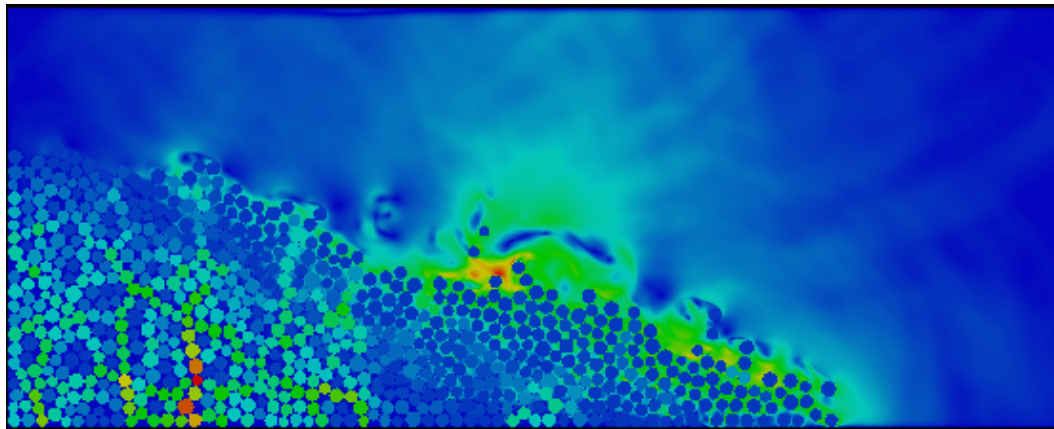
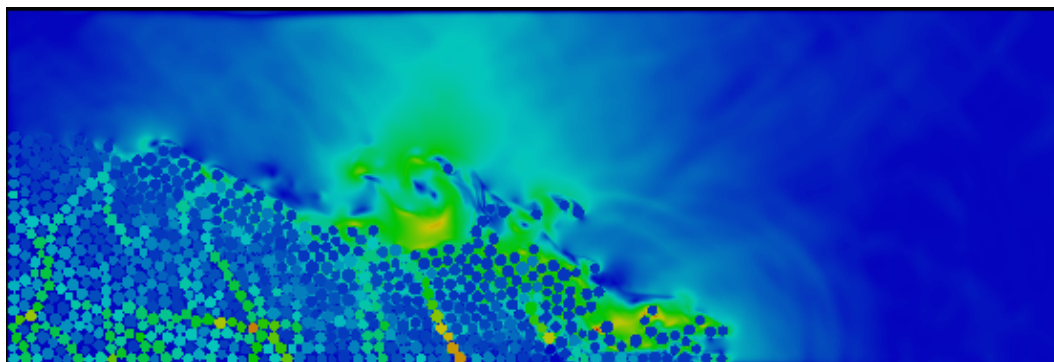


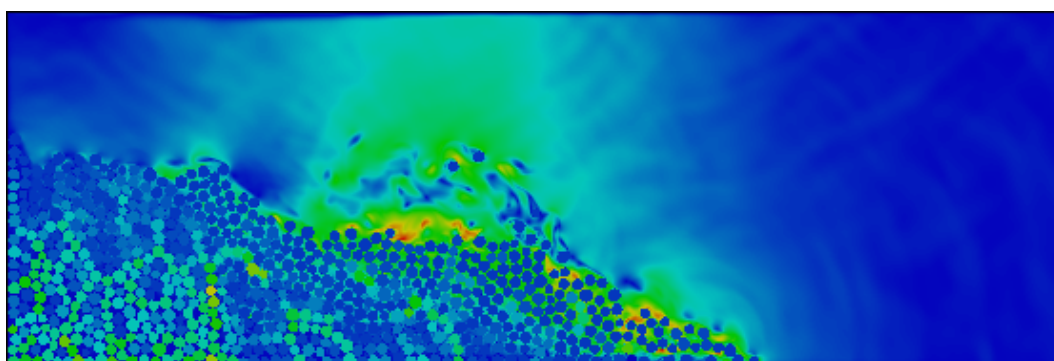
Figure 5.35 Evolution of run-out and kinetic energy with time (dense)



(a) Slope 2.5



(b) Slope 5.0



(c) Slope 7.5

Figure 5.36 Flow morphology at $t = 3\tau_c$ for different slope angles (dense)

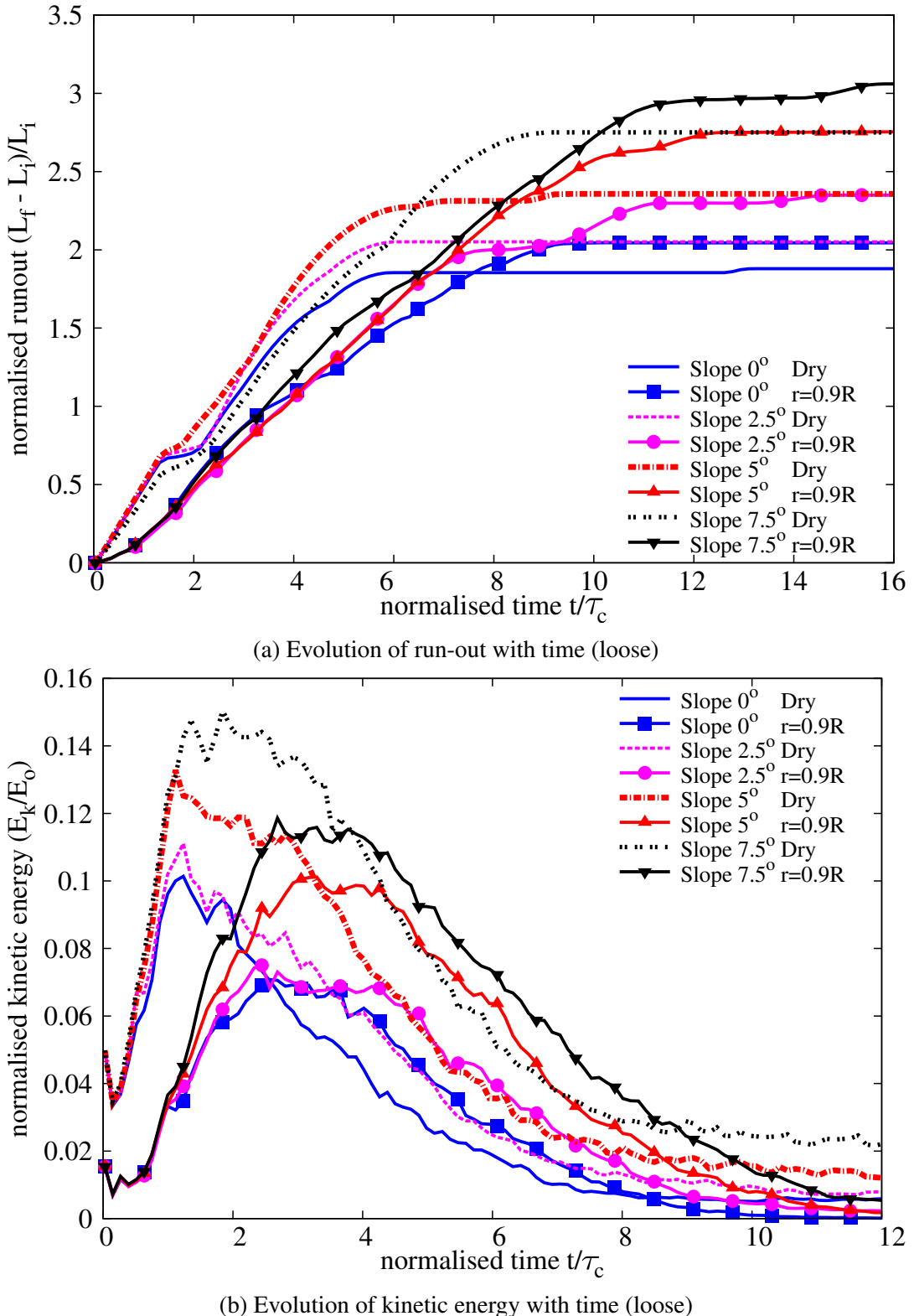
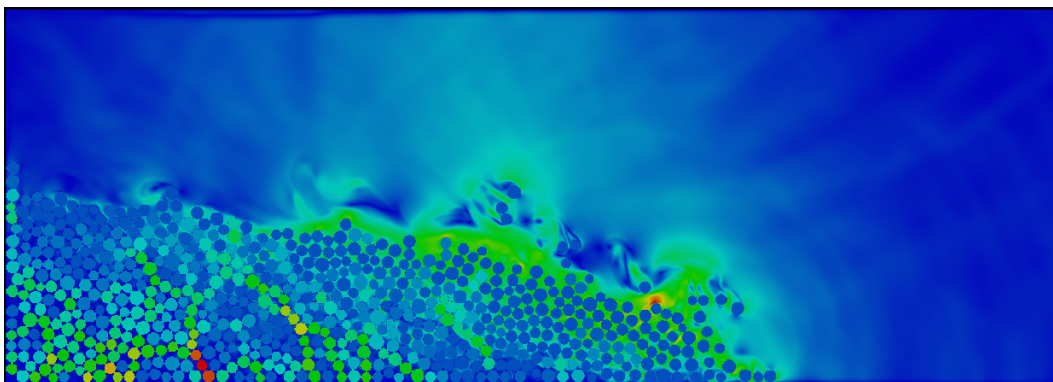


Figure 5.37 Evolution of run-out and kinetic energy with time (loose)

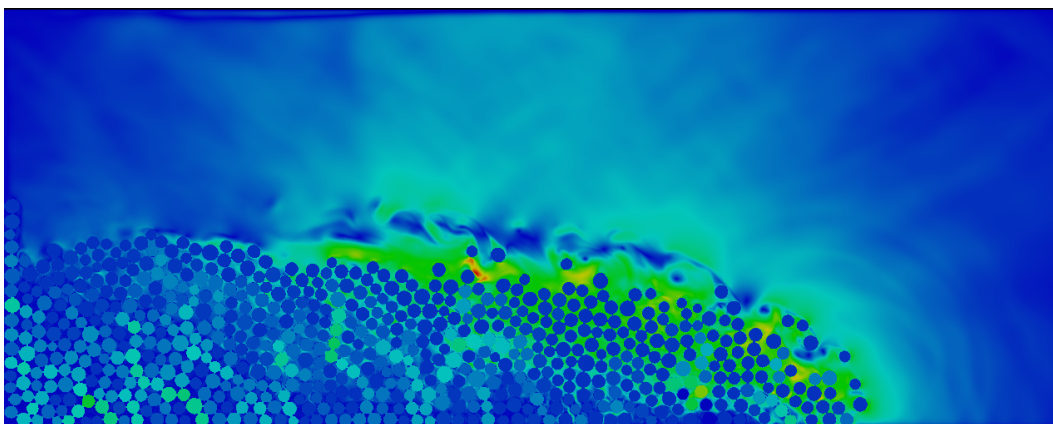
The snapshots at $t = 3\tau_c$ of a loose granular column ($a = 0.8$) collapse down slopes inclined at an angle of 2.5° , 5° and 7.5° are presented in figure 5.38. In contrast to dense granular flows, a plug-like flow can be observed. Due to the low permeability, the water entrapped in the flow front results in a drop in the density of the flowing mass thus enabling hydroplaning. The turbulence effect observed on the surface of the dense granular flow is absent in the loose granular collapse. This, along with the lubrication effect, results in a longer run-out distance in the submerged condition for a loose granular column than the dry collapse.

The evolution of packing density (figure 5.39) shows that, at the end of the flow, both the dense and the loose conditions reach similar packing density. This indicates that the dense granular column dilates more and is susceptible to higher viscous drag forces. Whereas in the loose condition, a positive pore-pressure is observed at the base of the flow, indicating entrainment of water at the base, i.e. lubrication and drop in the effective stress resulting in a longer run-out distance. The amount of water entrained in the loose granular column is higher than the dense condition, this can be observed by the low packing fraction observed between $2\tau_c$ and $5\tau_c$.

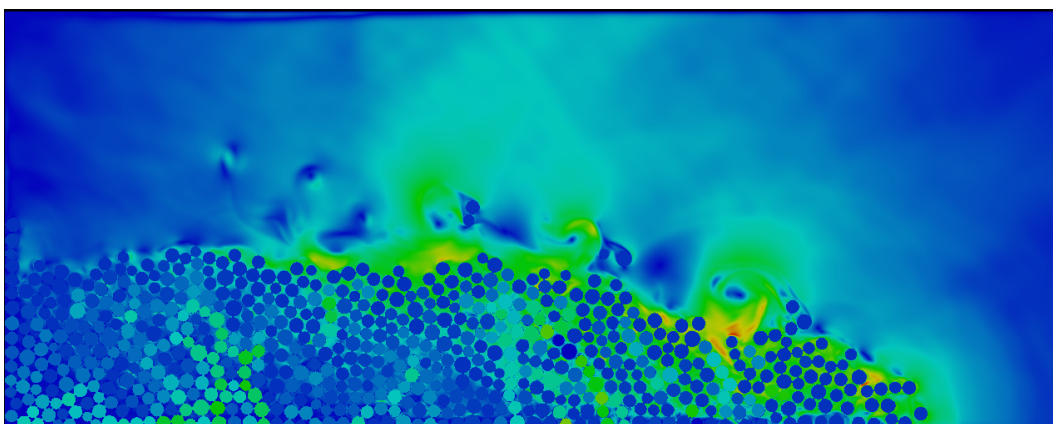
Figure 5.40a shows the evolution of run-out with slope angle for an initially dense granular column. With increase in the slope angle, the run-out increases in both dry and submerged conditions. For all slope angles, the run-out in the dry condition is higher than the submerged conditions. As the slope angle increases, the drag force experienced by the dense granular column predominates over the lubrication effect on the run-out behaviour, this results in an increase in the difference between the dry and the submerged conditions with increase in the slope angle. Whereas with increase in slope angle, the loose granular column flows longer than the dry conditions. The longer run-out in the loose granular column collapse is due to hydroplaning experienced at the flow front as a result of entrainment of water. Figure 5.41 shows that for a given initial aspect ratio and slope angle, the run-out distance in the loose granular collapse in fluid is higher than the dense condition. This observation in fluid is in contrast to the dry condition, where the dense granular column flows longer due to higher initial potential energy. The low permeability observed in the loose granular flow ensures that water entrained at the base of the flow front is retained resulting in sustained lubrication effect. Also, the low permeability ensures that the density of the flowing mass remains in a slurry state resulting in a longer duration of hydroplaning. These effects in the loose granular column with low permeability condition result in a longer run-out distance.



(a) Slope 2.5



(b) Slope 5.0



(c) Slope 7.5

Figure 5.38 Flow morphology at time $t = 3\tau_c$ for different slope angles (loose)

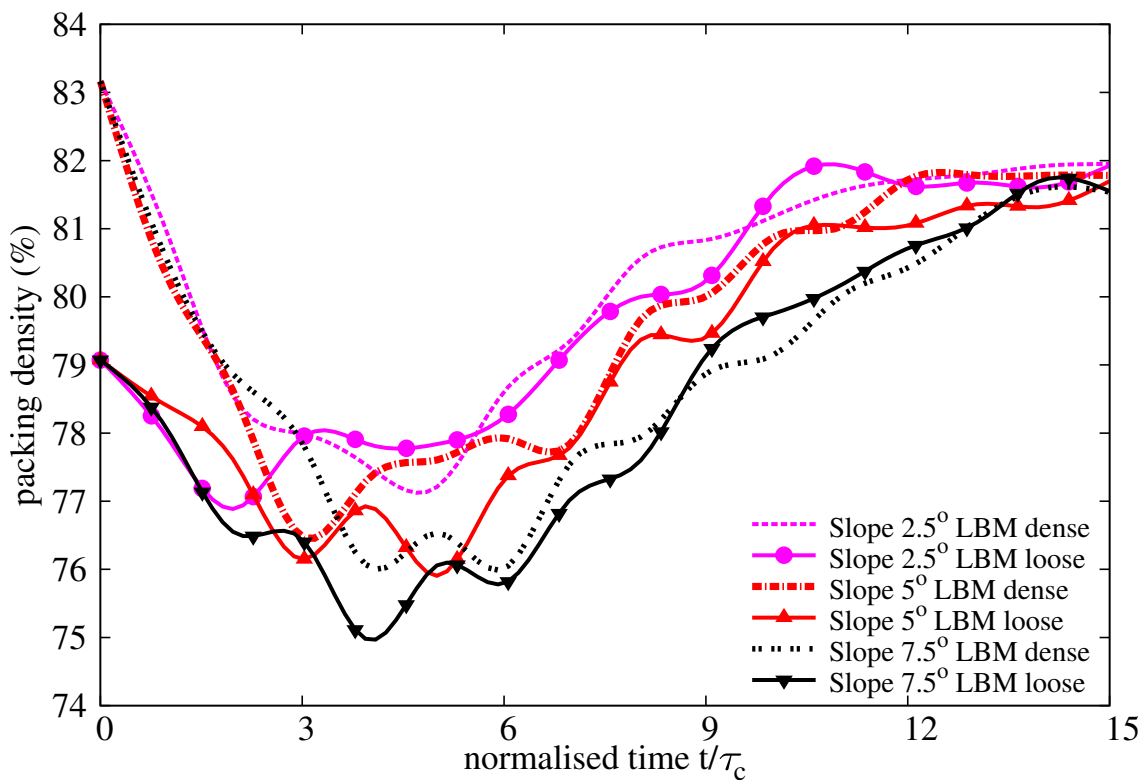
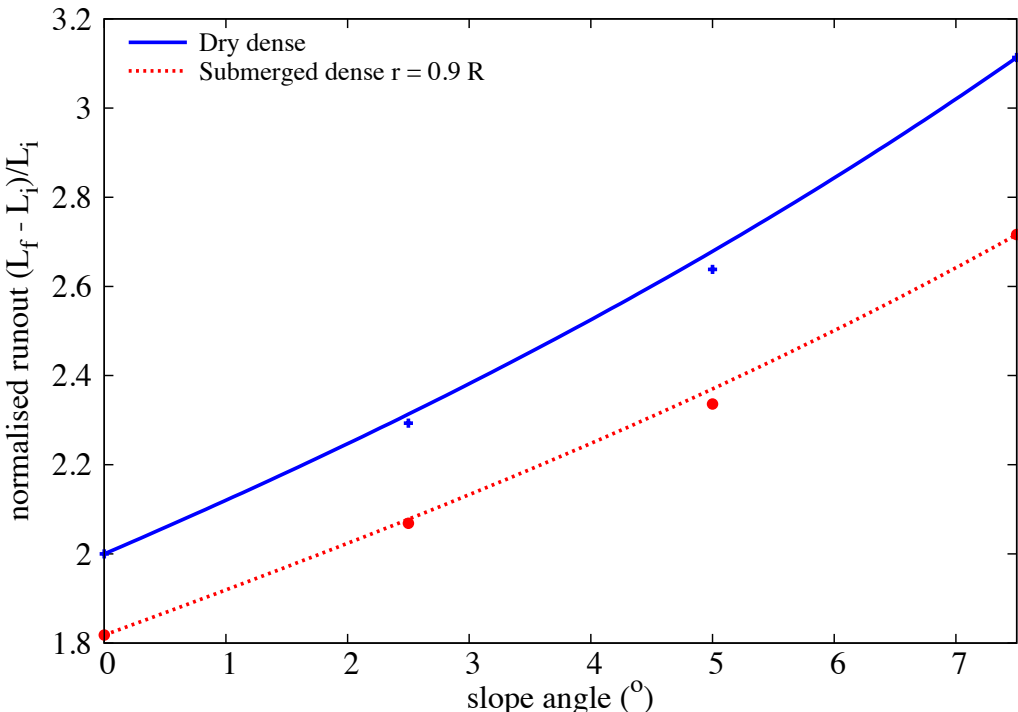
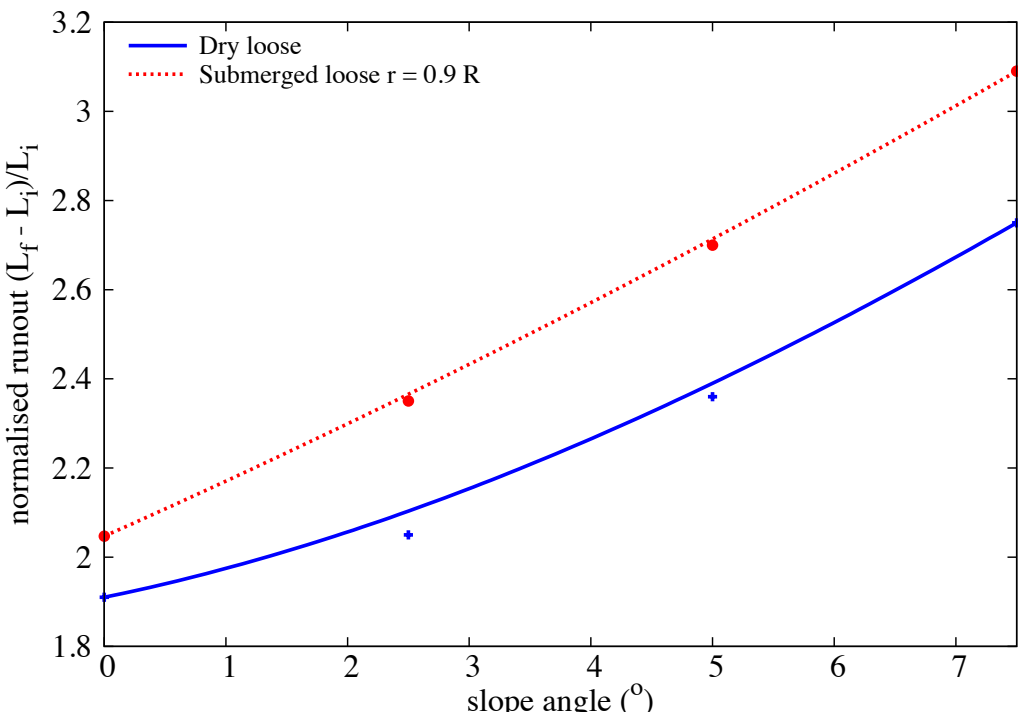


Figure 5.39 Evolution of packing density with time for different slope angles



(a) Dense



(b) Loose

Figure 5.40 Comparison between dry and submerged granular column on the effect of slope angle on the run-out distance (Dense and Loose).

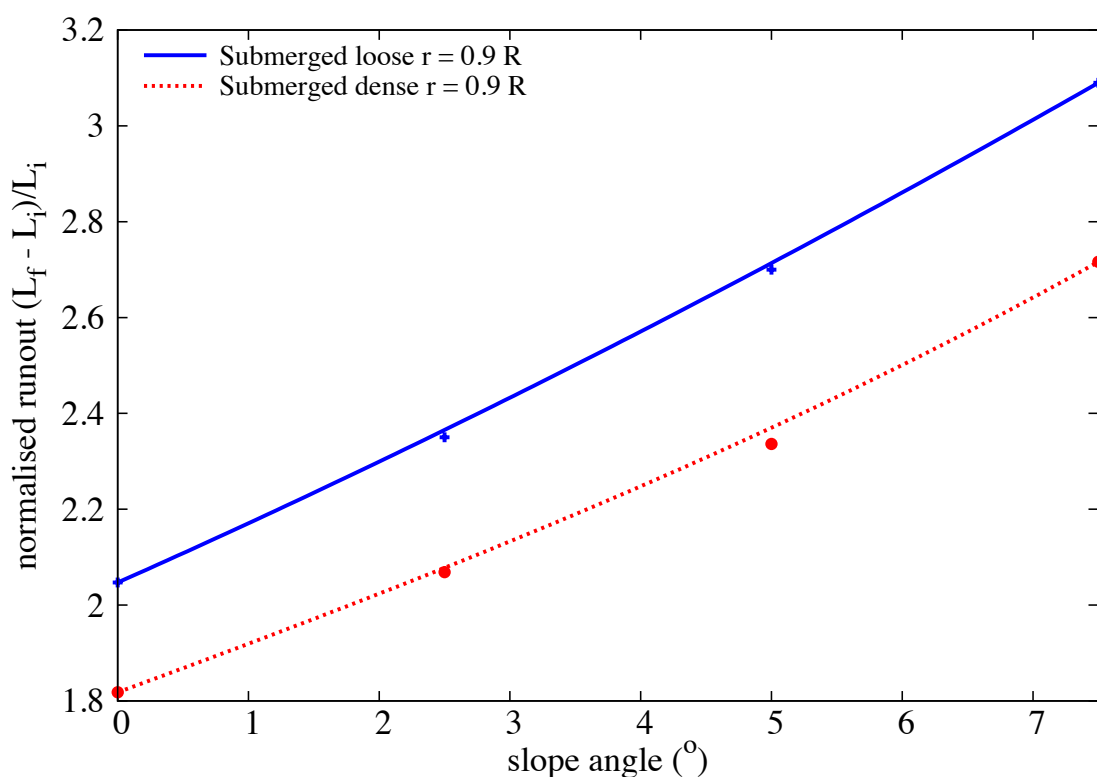


Figure 5.41 Effect of slope angle on the run-out behaviour for different initial packing density.

5.4.2 Effect of permeability

In order to understand the effect of permeability at a slope angle of 5° , the collapse of a granular column with an initial aspect ratio of 0.8 is simulated with different permeabilities. The hydrodynamic radius of a loosely packed granular column is varied from $r = 0.7 R$ (high permeability), $0.75 R$, $0.8 R$, $0.85 R$ to $0.9 R$ (low permeability). The run-out distance is found to increase with decrease in the permeability of the granular assembly (Figure 5.42a). The run-out distance for high permeable conditions ($r = 0.7 R - 0.8 R$) are lower than their dry counterparts. Although, decrease in permeability resulted in an increase in the run-out distance, no significant change in the run-out behaviour is observed for a hydrodynamic radius of up to $0.8 R$.

With further decrease in permeability ($r = 0.85 R$ and $0.9 R$), the run-out distance in the fluid is longer than that observed in the dry condition. At a very low permeability ($r = 0.9 R$), the flowing granular mass entrains more water at the base, which causes a reduction in the effective stress accompanied by a lubrication effect on the flowing granular media. This can be seen by a significant increase in the peak kinetic energy and the duration of the peak energy, in comparison to the dry and the highly permeable conditions (Figure 5.43a). However, the permeability of the granular column did not have an influence on the evolution of height during the flow. But, the dry granular column tends to collapse more than the immersed granular column due to lack of viscous dissipation (Figure 5.42b).

Positive pore-pressure generation at the base of the flow is observed for low permeable conditions. Inspection of the local packing density showed entrainment of water at the base of the flow, which can also be observed by the steep decrease in the packing density (Figure 5.43b) for the very low permeability condition ($r = 0.9 R$). At the end of the flow ($t \geq 10 \times \tau_c$), the excess pore-pressure dissipates and the granular flows, irrespective of their permeability, reach almost the same packing density.

Figure 5.45 shows the effect of permeability on the run-out behaviour for a dense and a loose granular column collapse on a slope of 5° and 0° . In both cases, the run-out distance increases with increase in the hydrodynamic radius (decrease in permeability). However in the dense case, the run-out distance observed in the fluid is shorter than the dry condition. Whereas in the loose condition, the run-out distance increases significantly at low permeabilities and results in a longer run-out distance in the submerged condition in comparison to the dry granular collapse. The comparison of loose and dense collapse on a slope of 0° and 5° shows that the initial packing density plays a significant role in the case of collapse on a horizontal plane, however at a slope of 5° , the run-out distance is unaffected by the initial packing density at high permeability conditions. This shows that at high permeabilities, the viscous drag forces predominate resulting in almost the same run-out

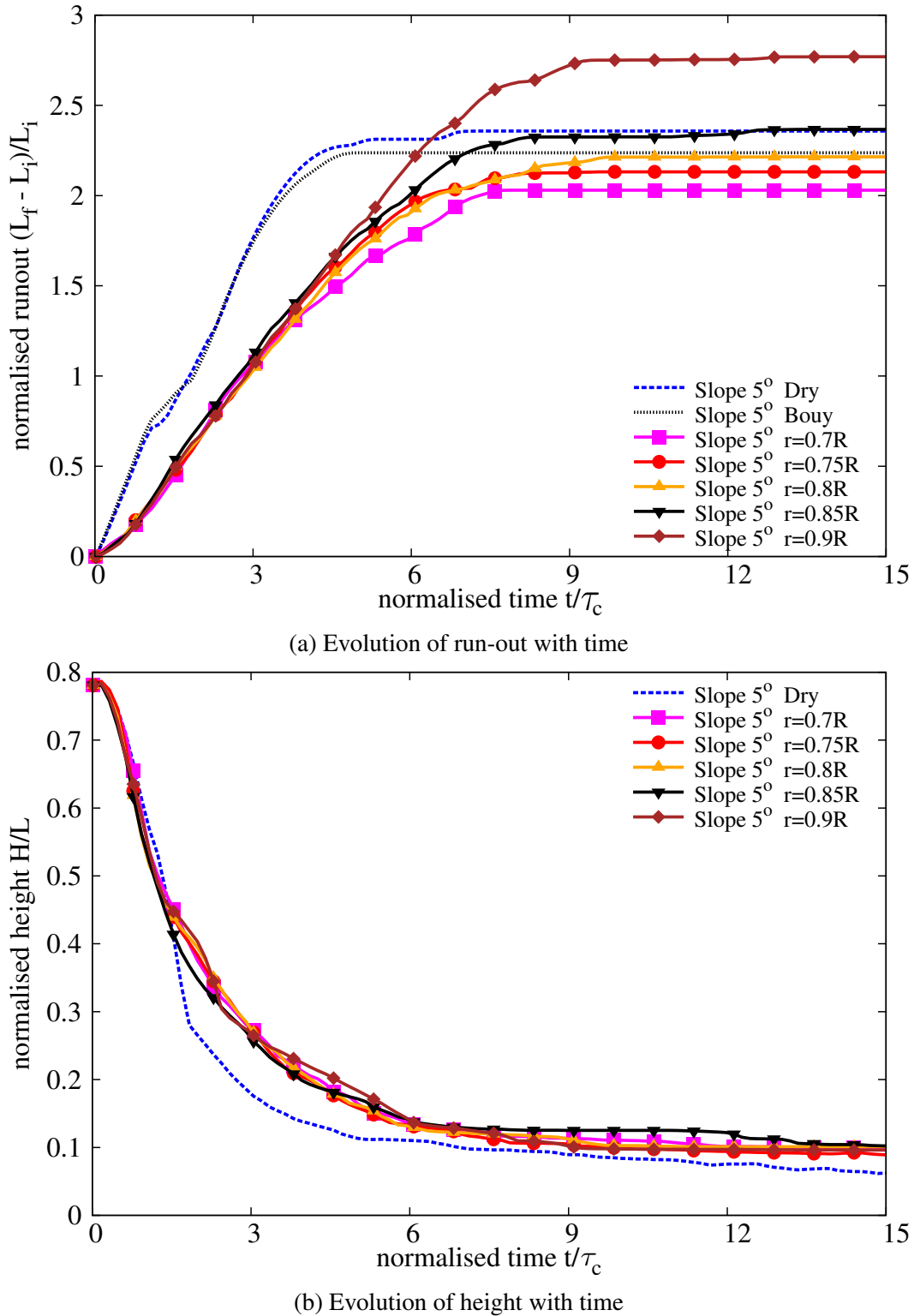


Figure 5.42 Evolution of run-out and height with time for different permeability (loose slope 5°)

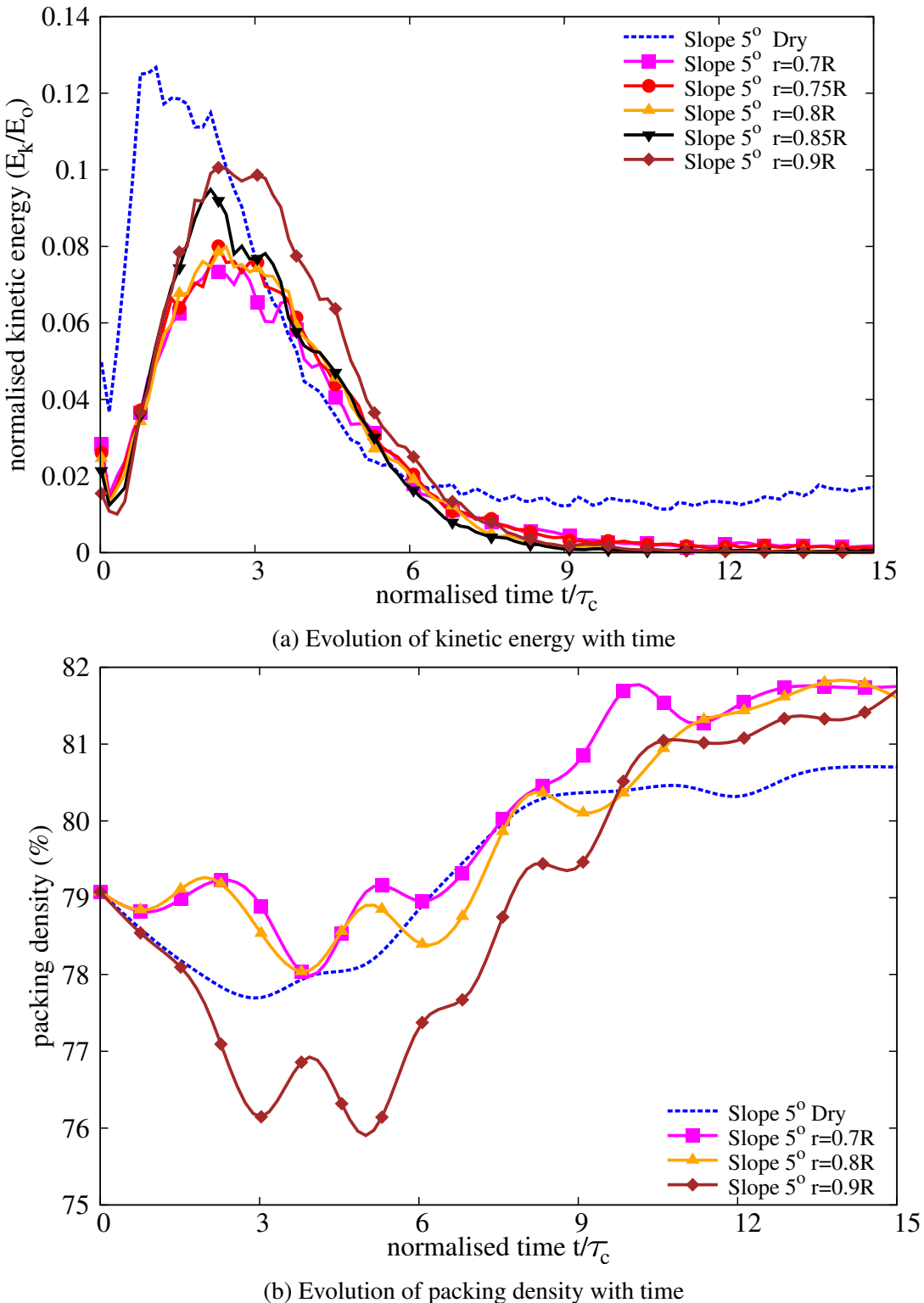


Figure 5.43 Evolution of kinetic energy and packing density with time for different permeability (loose slope 5°)

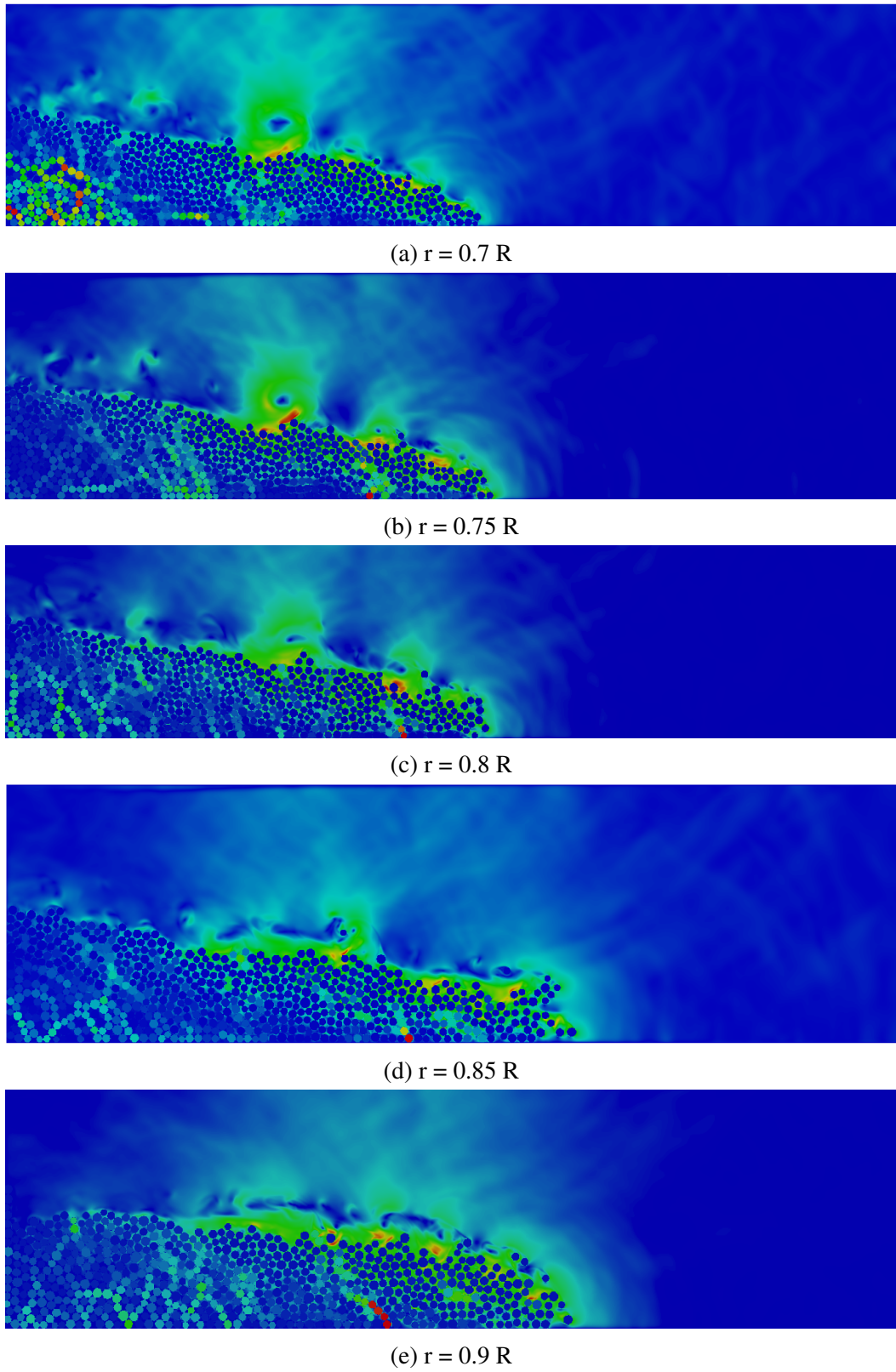


Figure 5.44 Evolution of the flow front at $t = 3\tau_c$ for different permeabilities (loose slope 5°).

distance for both dense and loose conditions. However at a low permeability ($r = 0.9 R$), hydroplaning is observed in the case of loose granular column resulting in a substantially longer run-out distance than the dense granular column in submerged condition.

5.5 Tall columns

In contrast to the collapse of short columns in fluid, the amount of material destabilised and in turn the surface area of the mobilised mass that interacts with the surrounding fluid increases. This increased interaction of the granular mass with the surrounding fluid results in the formation of turbulent vortices that alter the deposit morphology during the collapse. It was observed (section 5.3.2) that the vortices result in formation of heaps that significantly affects the distribution of mass in the flow. Staron and Hinch (2007) observed that the distribution of the mass in the granular flow plays a crucial role in the flow kinematics. In order to understand the behaviour of tall columns, the run-out behaviour of a dense granular column with an initial aspect ratio of 6 is studied. The collapse of a tall granular column on slopes of 0° , 2.5° , 5° and 7.5° are studied. A hydrodynamic radius of $r = 0.85 R$ is adopted. Unnatural permeability conditions were observed at higher hydrodynamic radii.

Snapshots of the collapse of an aspect ratio 6 column on a horizontal surface are shown in figure 5.47. The initial stage of collapse is characterised by the free-fall of grains above the failure surface. As the grains experience free-fall due to gravity, they interact with the surrounding fluid experiencing drag force. This results in a significant drop in the kinetic energy available for the flow. As the grains reach the static region, they interact with the neighbouring grains and the energy gained during the free fall is converted into horizontal acceleration. Uniquely during this stage ($t = 3\tau_c$) the interactions between the soil grains on the surface with the surrounding fluid result in the formation of eddies. The number of eddies formed during the flow is proportional to the surface area interacting with the fluid. Hydroplaning can be observed at the flow front ($t = 3\tau_c$). Two large vortices with almost the same size can be observed at the final stage of collapse. The soil grains on the surface experience suction due to formation of eddies and this results in formation of heaps of granular mass in front of each vortex. The formation of heaps, although in evidence, doesn't significantly affect the distribution of mass in the case of collapse on a horizontal plane.

Snapshots of the collapse of a granular column ($a = 6$) on a inclined plane at angle of 5° are shown in figure 5.48. Similar behaviour in the flow evolution is observed for the collapse on a slope of 5° . The vortices are formed only during the horizontal spreading stage $t = 3\tau_c$, but the number of vortices formed during the collapse is higher than the collapse on a horizontal plane. However, as the flow progresses a single large vortex engulfs other

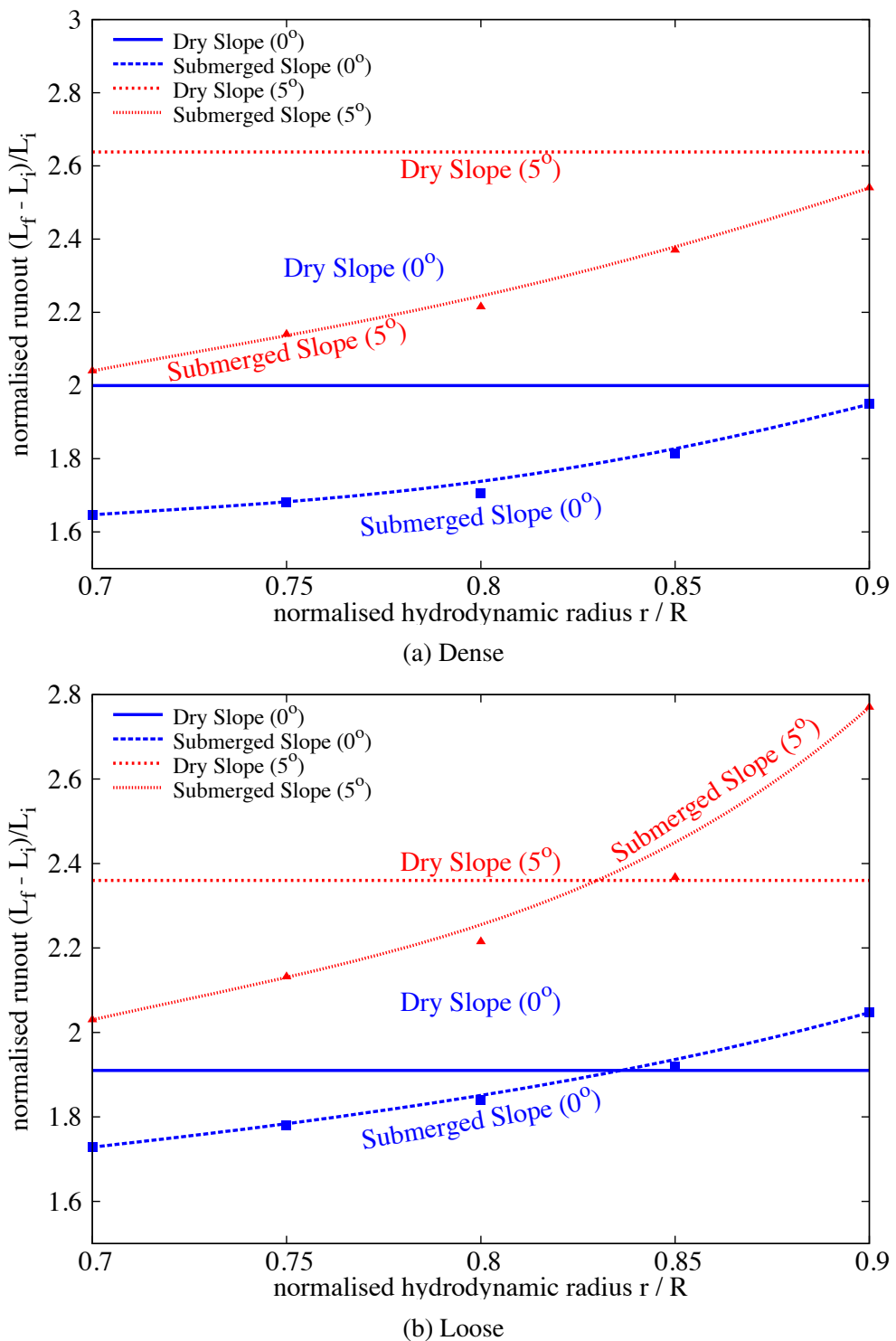


Figure 5.45 Comparison between dry and submerged granular column for a slope angle of 0° and 5° on the effect of permeability on the run-out distance (Dense and Loose).

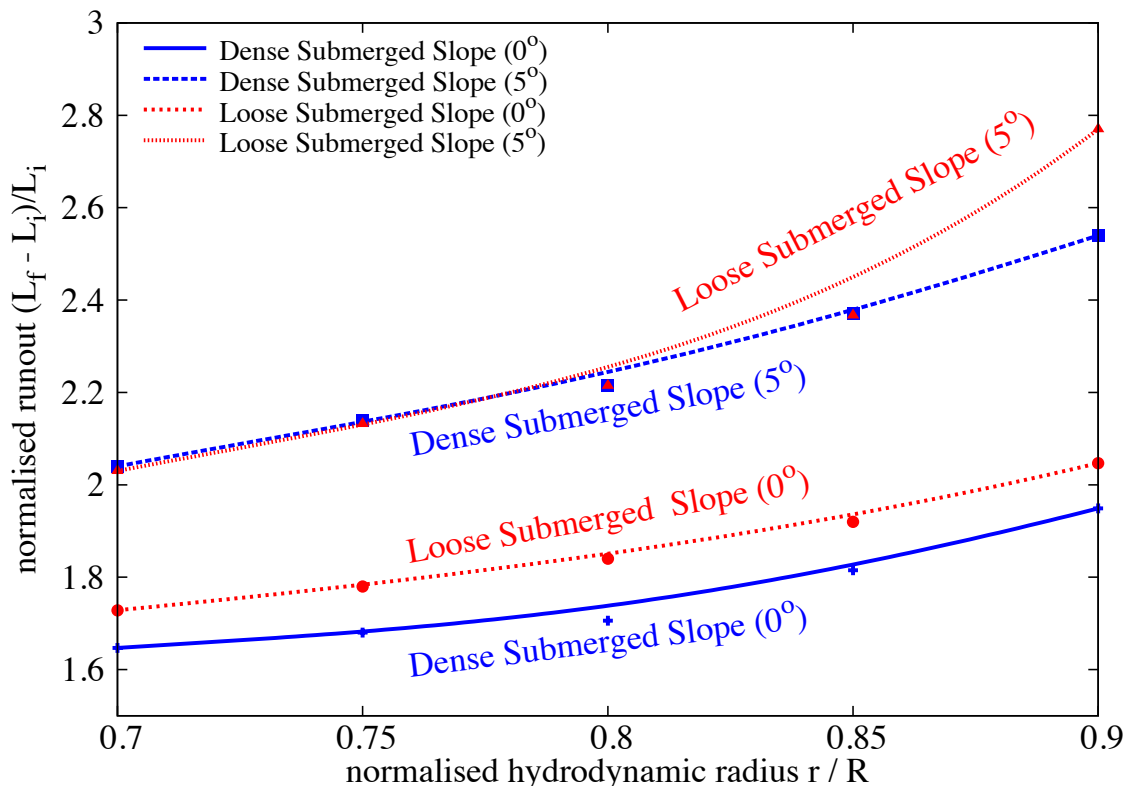


Figure 5.46 Effect of permeability on the run-out behaviour for different slope angle and the initial packing density.

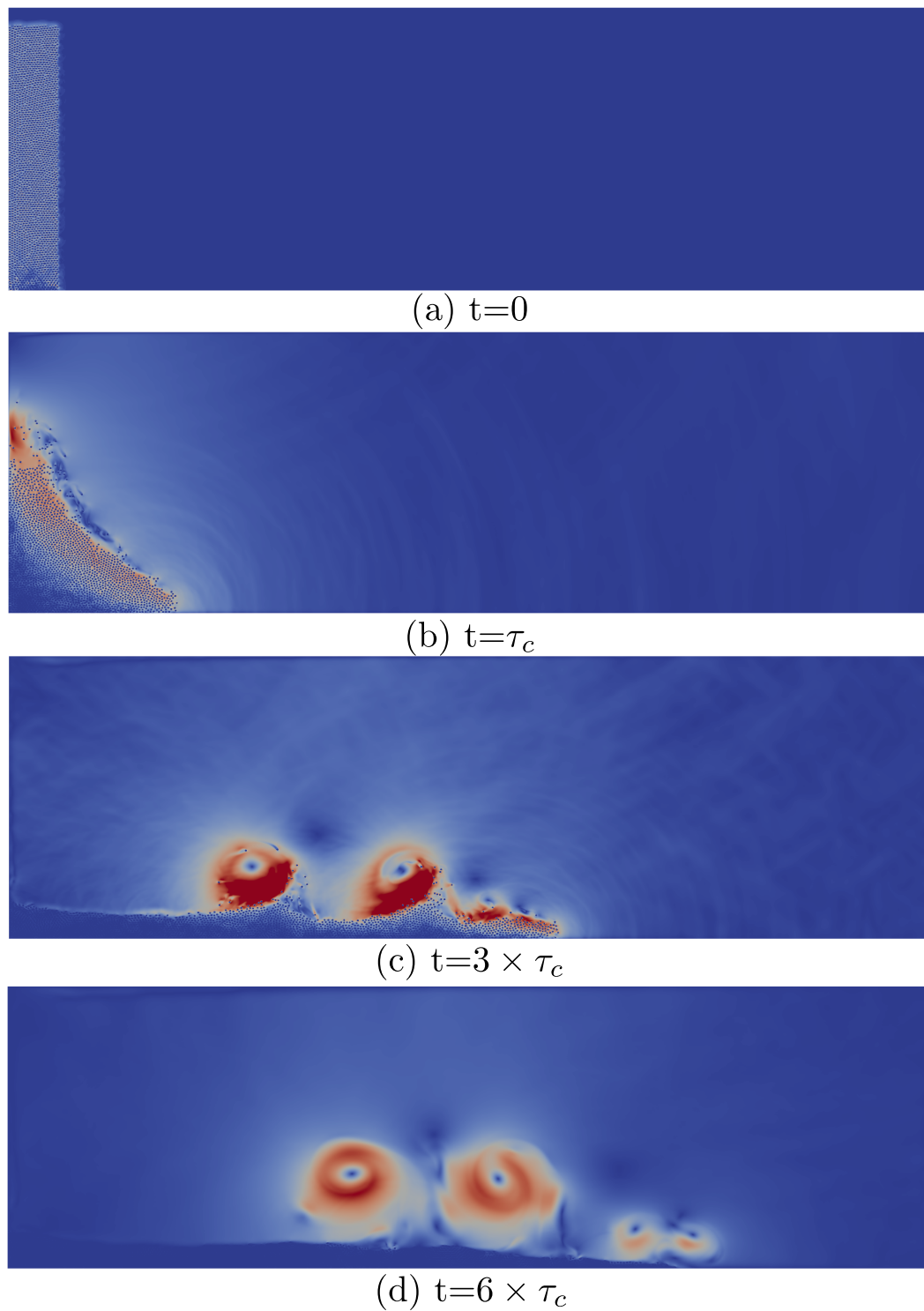


Figure 5.47 Flow evolution of a granular column collapse in fluid ($a = 6$) on a horizontal surface

smaller vortices, thus having a significant influence on the mass distribution. Figure 5.49 shows the distribution of mass and the packing density at $t = 6\tau_c$ and $t = 8\tau_c$. A heap can be observed in front of the large vortex almost at the middle of the flow. The height of the heap is higher than the collapse height next to the wall. However, when the flow comes to rest and the vortex moves away from the flowing surface, the mass present in the heap gets redistributed (as seen in $t = 8\tau_c$). This behaviour is significantly different from that observed in the case of short columns.

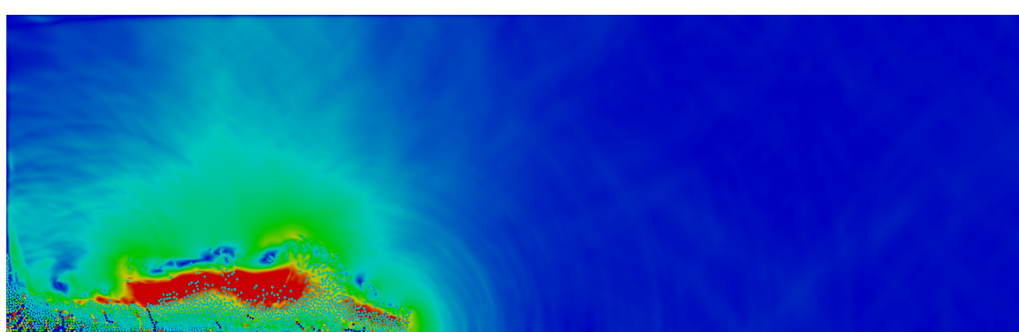
In order to understand the influence of slope angles on the run-out behaviour, the collapse of a granular column with an initial aspect ratio of 6 is performed on slopes of 0, 2.5°, 5° and 7.5°. The run-out evolution with time for different slope angles are presented in figure 5.50a. The run-out distance increases with increase in the slope angle, however the run-out distance in the fluid is significantly shorter than the dry condition. The slow evolution of run-out in the submerged condition is due to the delay in the dissipation of large negative pore-pressure developed during the initial stage of the collapse. The formation of eddies during the flow indicates that most of the potential energy gained during the free-fall is dissipated through viscous drag and formation of eddies. This effect predominates over the hydroplaning that is observed during the flow resulting in a shorter run-out distance in the case of fluid. The evolution of height with time indicates that the amount of material destabilised is much smaller due to the drag forces experienced by the grains (figure 5.50b).

The amount of kinetic energy available for the flow in the submerged condition is almost half that of the dry condition (figure 5.51a). It can be seen from figure 5.52b that the vertical kinetic energy is dissipate over a longer duration, in contrast to the free-fall release observed in the dry condition. The slower dissipation is attributed to the viscous drag force experienced by the grains and through formation of eddies.

The behaviour of tall columns are significantly different from that observed in the case of short columns. The slope angle has a strong influence on the number and size of eddies during the flow. The eddies interact with the surface of the granular flow and forms heaps in front of each vortex. This significantly affects the mass distribution and in turn the run-out evolution. Although, tall cliffs are quite rare in submarine condition in comparison to short cliffs or slopes, further research is required to understand the influence of permeability and packing density on the run-out evolution of tall columns.

5.6 Summary

Two-dimensional LB-DEM simulations are performed to understand the behaviour of submarine granular flows. Unlike dry granular collapse, the run-out behaviour in fluid is dictated

 $t = 0\tau_c$  $t = 1\tau_c$  $t = 3\tau_c$

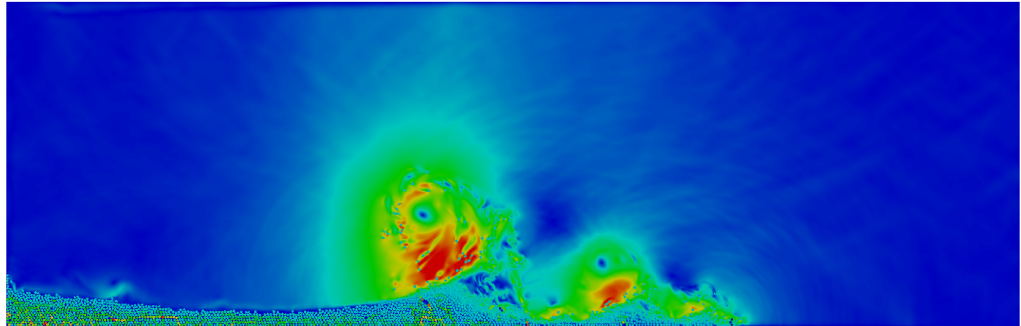
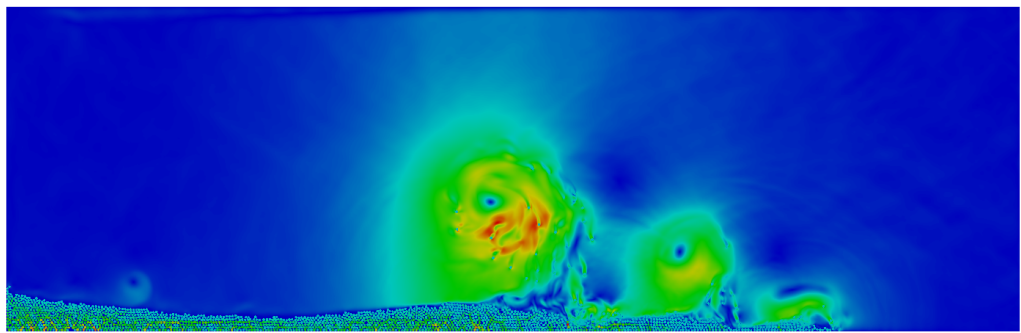
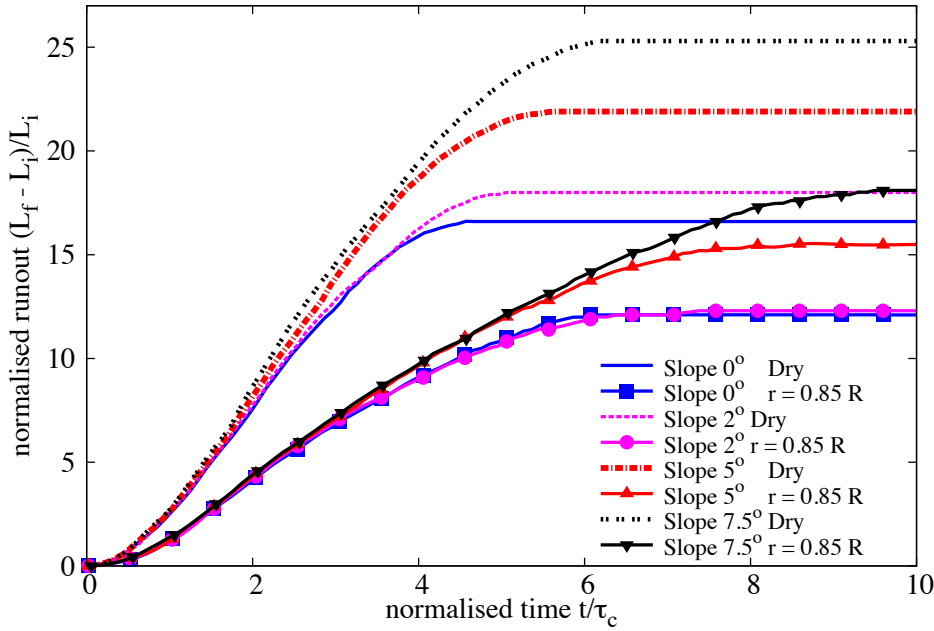
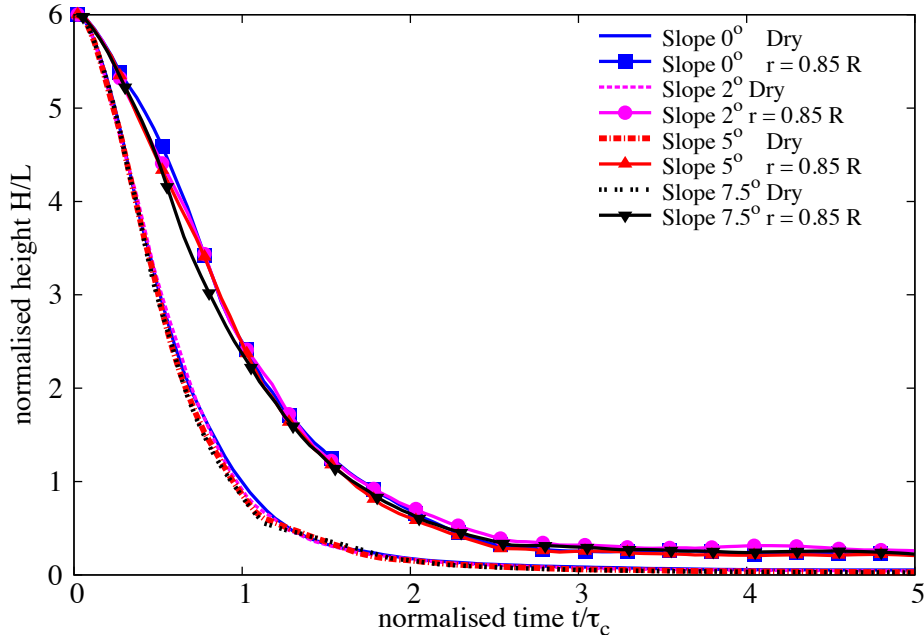
 $t = 6\tau_c$  $t = 8\tau_c$

Figure 5.48 Flow evolution of a granular column collapse in fluid ($a = 6$) on a slope of 5° . Shows the velocity profile of fluid due to interaction with the grains (red - higher velocity).

 $t = 6\tau_c$  $t = 8\tau_c$

Figure 5.49 Packing density of a granular column collapse in fluid ($a = 6$) on a slope of 5° .

(a) Evolution of run-out for a column collapse in fluid ($a = 6$) on a slope of 5° (b) Evolution of height with time for a column collapse in fluid ($a = 6$) on a slope of 5° Figure 5.50 Evolution of run-out and height for a column collapse in fluid ($a = 6$) on a slope of 5°

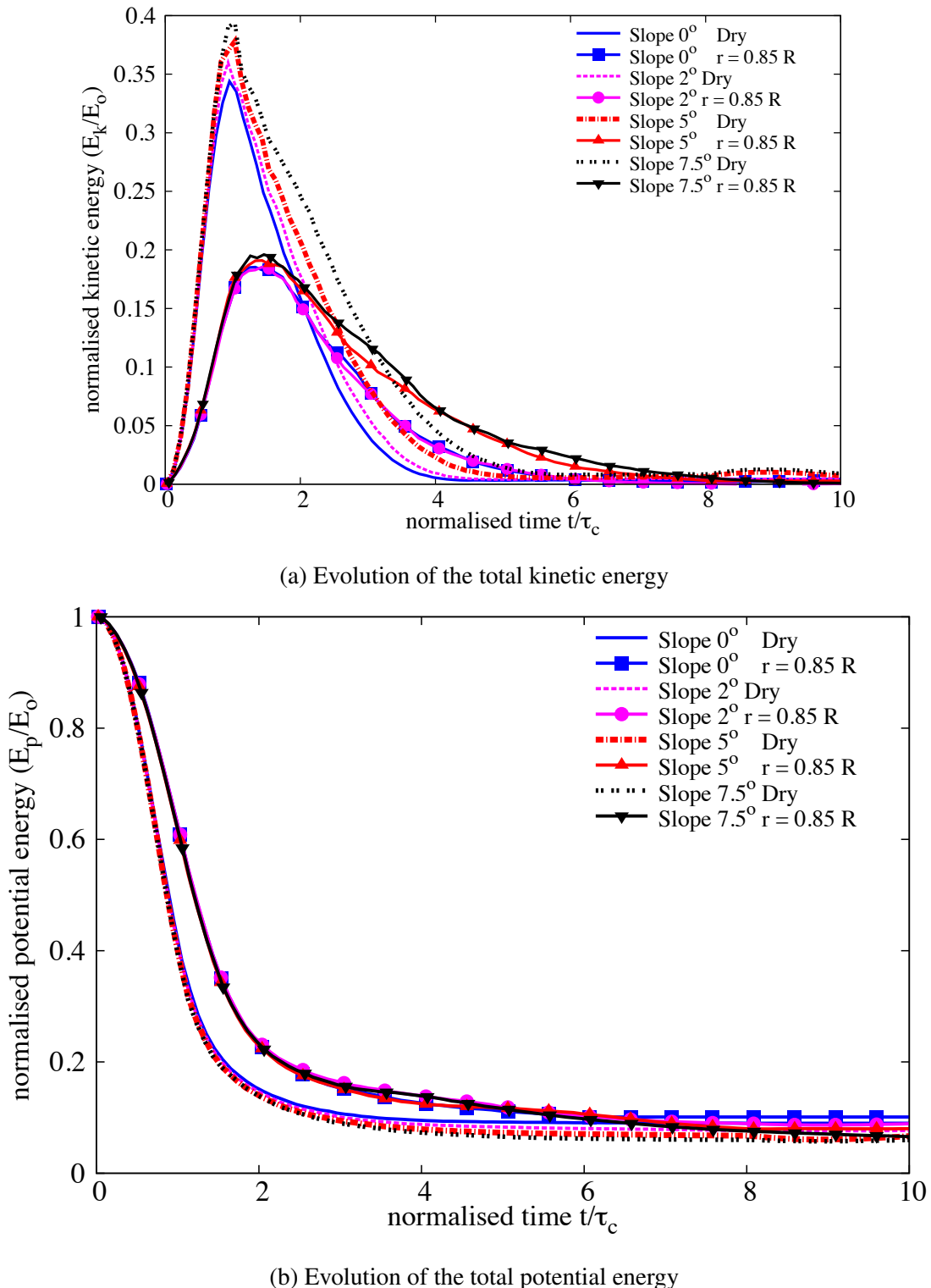
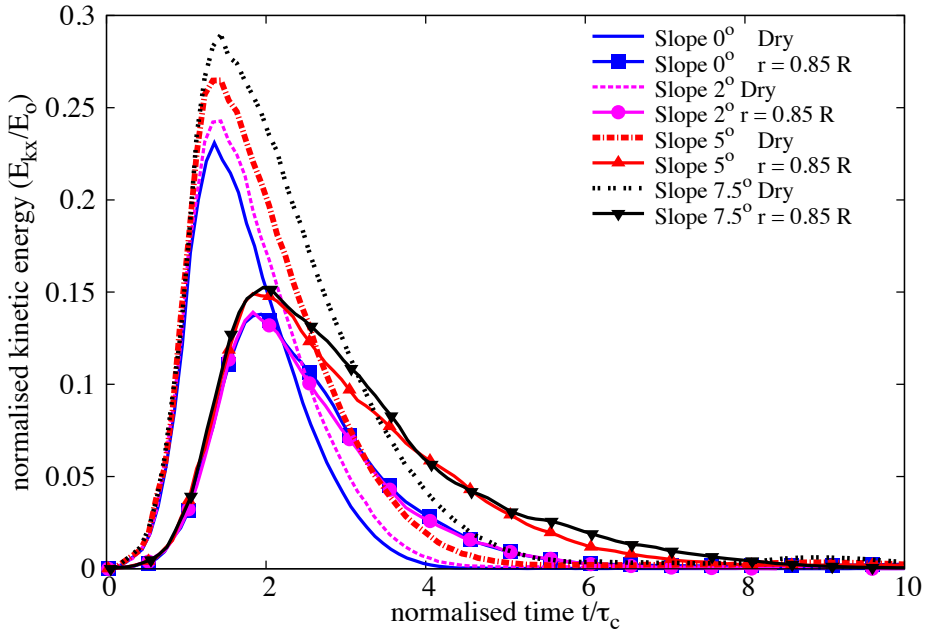
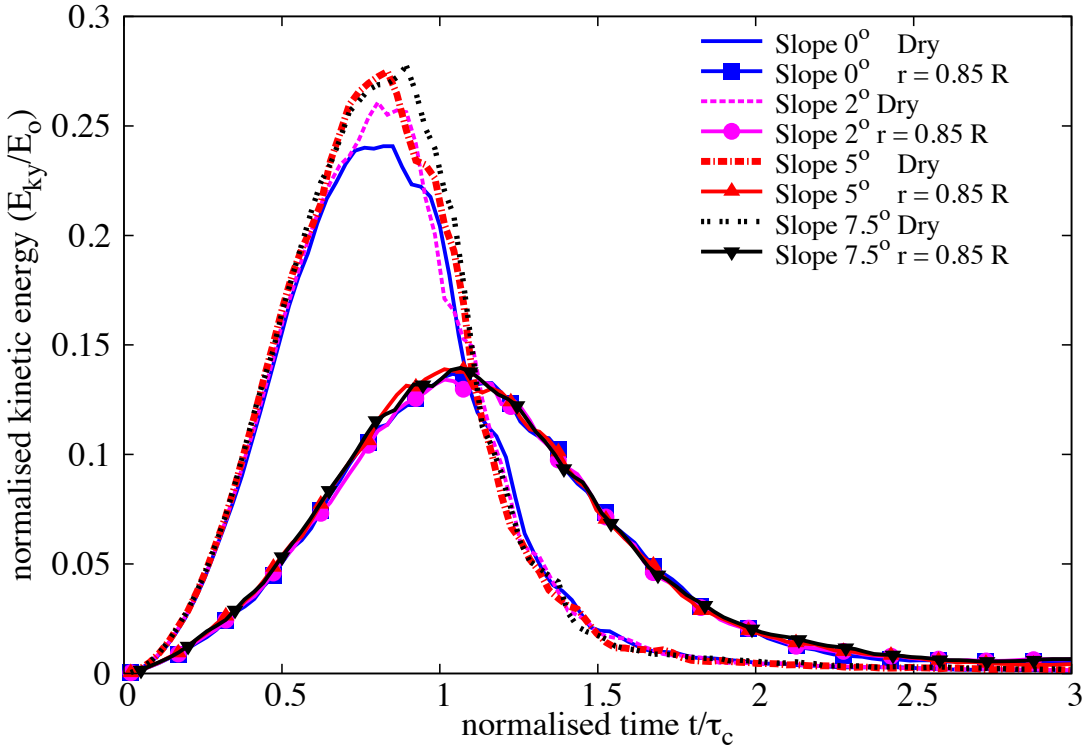


Figure 5.51 Evolution of the kinetic and the potential energy with time for a granular column collapse ($a = 6$) on a slope of 5°



(a) Evolution of the horizontal kinetic energy



(b) Evolution of the vertical kinetic energy

Figure 5.52 Evolution of the kinetic energies with time for a granular column collapse in fluid ($a = 6$) on a slope of 5°

by the initial volume fraction. Granular columns with loose packing and low permeability tend to flow further in comparison to dense columns, due to entrainment of water at the base resulting in lubrication. In both dense and loose conditions, the run-out distance increases with decrease in the permeability. With decrease in permeability, the duration required for the flow to initiate takes longer due to the development of large negative pore-pressure. However, the low permeability of the granular mass results in entrainment of water causing hydroplaning. For the same thickness and velocity of the flow, the potential of hydroplaning is influenced by the density of the flowing mass. Loose columns are more likely to hydroplane than the dense granular masses. The loose columns entrain more water at the flow front, leading to a partial fluidisation of the material. Thus resulting in a longer run-out distance than the dry condition. However, with increase in the slope angle, the run-out in fluid is influenced by the viscous drag acting on the granular materials more than the lubrication effect.

References

- Abe, K., Soga, K., and Bandara, S. (2013). Material Point Method for Coupled Hydromechanical Problems. *Journal of Geotechnical and Geoenvironmental Engineering*.
- Balmforth, N. J. and Kerswell, R. R. (2005). Granular collapse in two dimensions. *Journal of Fluid Mechanics*, 538:399–428.
- Bandara, S. (2013). *Material Point Method to simulate Large Deformation Problems in Fluid-saturated Granular Medium*. PhD thesis, University of Cambridge.
- Bardenhagen, S. and Kober, E. (2004). The generalized interpolation material point method. *Computer Modeling in Engineering and Sciences*, 5(6):477–496.
- Cambou, B., Jean, M., and Radjaï, F. (2009). *Micromechanics of granular materials*. Wiley-ISTE.
- Crosta, G. B., Imposimato, S., and Roddeman, D. (2009). Numerical modeling of 2-D granular step collapse on erodible and nonerodible surface. *Journal of Geophysical Research*, 114(F3):F03020.
- Da Cruz, F., Emam, S., Prochnow, M., Roux, J. N., and Chevoir, F. (2005). Rheophysics of dense granular materials: Discrete simulation of plane shear flows. *Physical Review E - Statistical, Nonlinear, and Soft Matter Physics*, 72(2):1–17.
- Daerr, A. and Douady, S. (1999). Two types of avalanche behaviour in granular media. *Nature*, 399(6733):241–243.
- Dey, R., Hawlader, B., Philips, R., and Soga, K. (2012). Effects of Shear Band Propagation on Submarine Landslide. In *Proceedings of the twenty-second International Offshore and Polar Engineering Conference*, Greece. e International Society of Offshore and Polar Engineers (ISOPE).
- Estrada, N., Taboada, A., and Radjai, F. (2008). Shear strength and force transmission in granular media with rolling resistance. *Physical Review E*, 78(2):021301.
- Girolami, L., Hergault, V., Vinay, G., and Wachs, A. (2012). A three-dimensional discrete-grain model for the simulation of dam-break rectangular collapses: comparison between numerical results and experiments. *Granular Matter*, pages 1–12.
- Guilkey, J., Harman, T., Xia, A., Kashiwa, B., and McMurtry, P. (2003). An Eulerian-Lagrangian approach for large deformation fluid structure interaction problems, Part 1: algorithm development. *Advances in Fluid Mechanics*, 36:143–156.

- Hogg, A. J. (2007). Two-dimensional granular slumps down slopes. *Physics of Fluids*, 19(9):9.
- Iverson, R. M. (1997). The physics of debris flows. *Rev. Geophys.*, 35(3):245–296.
- Jean, M. (1999). The non-smooth contact dynamics method. *Computer Methods in Applied Mechanics and Engineering*, 177(3-4):235–257.
- Kerswell, R. (2005). Dam break with Coulomb friction: A model for granular slumping? *Physics of Fluids*, 17:057101.
- Lajeunesse, E., Mangeney-Castelnau, A., and Vilotte, J. P. (2004). Spreading of a granular mass on a horizontal plane. *Physics of Fluids*, 16(7):2371.
- Lajeunesse, E., Monnier, J. B., and Homsy, G. M. (2005). Granular slumping on a horizontal surface. *Physics of Fluids*, 17(10).
- Larrieu, E., Staron, L., and Hinch, E. J. (2006). Raining into shallow water as a description of the collapse of a column of grains. *Journal of Fluid Mechanics*, 554:259–270.
- Lo, C. Y., Bolton, M., and Cheng, Y. P. (2009). Discrete element simulation of granular column collapse. In *AIP Conf. Proc. Powders and Grains 2009*, volume 1145 of *6th International Conference on Micromechanics of Granular Media, Powders and Grains 2009*, pages 627–630.
- Lube, G., Huppert, H. E., Sparks, R. S. J., and Freundt, A. (2005). Collapses of two-dimensional granular columns. *Physical Review E - Statistical, Nonlinear, and Soft Matter Physics*, 72(4):1–10.
- Mast, C. M., Arduino, P., Mackenzie-Helnwein, P., and Miller, G. R. (2014). Simulating granular column collapse using the Material Point Method. *Acta Geotechnica*.
- Mitchell, J. K. and Soga, K. (2005). *Fundamentals of soil behavior*. John Wiley & Sons.
- Moreau, J. J. (1993). New computation methods in granular dynamics. In Thornton, C., editor, *Powders and Grains*, page 227. A. A. Balkema.
- Mutabaruka, P. (2013). *Modélisation numérique des milieux granulaires immergés : initiation et propagation des avalanches dans un fluide*. Phd thesis, University of Montpellier 2.
- Radjai, F. and Dubois, F. (2011). *Discrete-element modeling of granular materials*. ISTE Wiley, London; Hoboken, N.J.
- Radjai, F. and Richefeu, V. (2009). Contact dynamics as a nonsmooth discrete element method. *Mechanics of Materials*, 41(6):715–728.
- Radjai, F., Schafer, J., Dipple, S., and Wolf, D. (1997). Collective Friction of an Array of Particles: A Crucial Test for Numerical Algorithms. *Journal de Physique I*, 7(9):1053–1070.
- Rondon, L., Pouliquen, O., and Aussillous, P. (2011). Granular collapse in a fluid: Role of the initial volume fraction. *Physics of Fluids*, 23(7):073301–073301–7.

- Rycroft, C. H., Orpe, A. V., and Kudrolli, A. (2009). Physical test of a particle simulation model in a sheared granular system. *Physical Review E*, 80(3):031305.
- Staron, L. and Hinch, E. J. (2007). The spreading of a granular mass: Role of grain properties and initial conditions. *Granular Matter*, 9(3-4):205–217.
- Staron, L., Radjai, F., and Villette, J. P. (2005). Multi-scale analysis of the stress state in a granular slope in transition to failure. *The European physical journal. E, Soft matter*, 18(3):311–20.
- Topin, V., Monerie, Y., Perales, F., and Radjaï, F. (2012). Collapse Dynamics and Runout of Dense Granular Materials in a Fluid. *Physical Review Letters*, 109(18):188001.
- Utili, S., Zhao, T., and Houlsby, G. (2014). 3D DEM investigation of granular column collapse: Evaluation of debris motion and its destructive power. *Engineering Geology*.
- Warnett, J. M., Denissenko, P., Thomas, P. J., Kiraci, E., and Williams, M. A. (2013). Scalings of axisymmetric granular column collapse. *Granular Matter*, 16(1):115–124.
- Zenit, R. (2005). Computer simulations of the collapse of a granular column. *Physics of Fluids*, 17(Compendex):031703–1–031703–4.